

REACTION KINETICS OF CALCIUM CHLORIDE - AMMONIA REACTIVE
SYSTEM AND THEORETICAL SIMULATION OF HEAT AND MASS
TRANSFER IN POROUS SLAB PELLETS

A THESIS SUBMITTED TO
THE GRADUATE SCHOOL OF NATURAL AND APPLIED SCIENCES
OF
MIDDLE EAST TECHNICAL UNIVERSITY

BY

ZEYNEP KARAKAŞ HELVACI

IN PARTIAL FULFILLMENT OF THE REQUIREMENTS
FOR
THE DEGREE OF DOCTOR OF PHILOSOPHY
IN
CHEMICAL ENGINEERING

JANUARY 2023

Approval of the thesis:

**REACTION KINETICS OF CALCIUM CHLORIDE - AMMONIA
REACTIVE SYSTEM AND THEORETICAL SIMULATION OF HEAT
AND MASS TRANSFER IN POROUS SLAB PELLETS**

submitted by **ZEYNEP KARAKAŞ HELVACI** in partial fulfillment of the requirements for the degree of **Doctor of Philosophy in Chemical Engineering, Middle East Technical University** by,

Prof. Dr. Halil Kalıpçılar
Dean, Graduate School of **Natural and Applied Sciences** _____

Prof. Dr. Pınar Çalık
Head of the Department, **Chemical Engineering** _____

Prof. Dr. Yusuf Uludağ
Supervisor, **Chemical Engineering, METU** _____

Prof. Dr. Gürkan Karakaş
Co-Supervisor, **Chemical Engineering, METU** _____

Examining Committee Members:

Prof. Dr. Levent Yılmaz
Chemical Engineering, METU _____

Prof. Dr. Yusuf Uludağ
Chemical Engineering, METU _____

Prof. Dr. Suna Balcı
Chemical Engineering, Gazi University _____

Prof. Dr. Nihal Aydoğan
Chemical Engineering, Hacettepe University _____

Assoc. Prof. Dr. Özgür Bayer
Mechanical Engineering, METU _____

Date: 24.01.2023

I hereby declare that all information in this document has been obtained and presented in accordance with academic rules and ethical conduct. I also declare that, as required by these rules and conduct, I have fully cited and referenced all material and results that are not original to this work.

Name Last name : Zeynep Karakaş Helvacı

Signature :

ABSTRACT

REACTION KINETICS OF CALCIUM CHLORIDE - AMMONIA REACTIVE SYSTEM AND THEORETICAL SIMULATION OF HEAT AND MASS TRANSFER IN POROUS SLAB PELLETS

Karakaş Helvacı, Zeynep
Doctor of Philosophy, Chemical Engineering
Supervisor : Prof. Dr. Yusuf Uludağ
Co-Supervisor: Prof. Dr. Gürkan Karakaş

January 2023, 146 pages

The reactive systems between ammoniated CaCl_2 and NH_3 were investigated in terms of heat and mass transport phenomena coupled with reaction kinetics. The reversible reaction rate based on the Langmuir-Hinshelwood model was suggested to express the net reaction rate, including both the adsorption and desorption terms. Experiments at three temperatures were conducted to evaluate the kinetic parameters, pre-exponential factors, and activation energies. The parameters were evaluated by Non-Linear Regression (NLR) analysis using the Polymath software. Experiments with 0.3 grams of initial metal salt results were used for the reaction between two- and four- ammoniated CaCl_2 in NLR analysis. Calculated reaction rates were also compared with the experimental result obtained from the 0.5 grams of initial CaCl_2 . Pre-exponential factors were obtained as $7.06 \cdot 10^{-22} \text{min}^{-1} \text{bar}^{-3}$ and 102min^{-1} for adsorption and desorption terms, respectively. Also, apparent adsorption and desorption activation energies were obtained as $-115600 \text{J mol}^{-1}$ and 23310J mol^{-1} , respectively. The calculated and experimental results showed well agreement. The parameters for the reaction between four- and eight-ammoniated CaCl_2 were obtained by the 0.5 grams of initial CaCl_2 experiments. Pre-exponential

factors for adsorption and desorption reactions were obtained as $2.64 \cdot 10^{-18} \text{ min}^{-1} \text{ bar}^{-3}$ and 3.44 min^{-1} , respectively. Also, apparent adsorption and desorption activation energies were obtained as $-88130 \text{ J mol}^{-1}$ and 16500 J mol^{-1} for the adsorption and desorption terms. The negative activation energies in both reactions indicated the complex reactions in the reaction mechanism.

Since CaCl_2 is used in the pellet forms in the Chemical Heat Pump and hydrogen storage applications, a theoretical model was developed taking into account heat and mass transport phenomena with the consideration of chemical reaction rate. As a contribution to the literature, volume increase was integrated into the model, and the developed reversible reaction rate expression was used. In order to compare the simulation results, slab pellet experiments were also conducted in the same experimental setup. The simulation change in bulk ammonia pressure was compared with the experimental results. The results were in agreement for the reaction between two- and four-ammoniated CaCl_2 in the first 700 seconds. The deviation beyond this time may be the constant effective diffusivity assumption in the model. The effective diffusivities of the reactive systems were assumed according to the literature and assumed as constant during the reaction, while it was thought that it was changing during the experiment. Moreover, the experimental and simulation results showed well agreement for the reaction between four- and eight-ammoniated CaCl_2 . The deviation observed in the former case was not seen in the latter case. This was attributed to the fact that at the end of the experiment, the slab pellet structure integrity disappeared, and the pellet dispersed. Therefore, the effective diffusivity might not decrease during the experiments, which was compatible with the simulation assumption.

Keywords: Chemical Heat Pump, Hydrogen Storage, Reaction Kinetics, Solid-gas reactions, $\text{CaCl}_2\text{-NH}_3$

ÖZ

KALSİYUM KLORÜR - AMONYAK REAKTİF SİSTEMİN REAKSİYON KİNETİKLERİ VE GÖZENEKLİ LEVHA FORMUNDA PELLETLERİN ISI VE KÜTLE TRANSFERLERİNİN TEORİK SİMÜLASYONU

Karakaş Helvacı, Zeynep
Doktora, Kimya Mühendisliği
Tez Yöneticisi: Prof. Dr. Yusuf Uludağ
Ortak Tez Yöneticisi: Prof. Dr. Gürkan Karakaş

Ocak 2023, 146 sayfa

Amonyaklı metal tuzları ve amonyak reaktif sistemleri ısı ve kütle transferi de dikkate alınarak reaksiyon kinetiği açısından incelenmiştir. Net reaksiyon hızını ifade edebilmek için, Langmuir-Hinshelwood modeli temel alan, adsorpsiyon ve desorpsiyon reaksiyonlarını birlikte değerlendiren, bir tersinir reaksiyon mekanizması önerilmiştir. Kinetik parametreleri, ön ekspanansiyel faktörleri ve aktivasyon enerjilerini hesaplayabilmek için üç farklı sıcaklıkta deneyler gerçekleştirilmiştir. Bu parametreler lineer olmayan regresyon analizi (NLR) ile Polymath yazılımında hesaplanmıştır. İki amonyak ve dört amonyak bağlı CaCl_2 tuzları arasında meydana gelen reaksiyonun parametreleri için 0.3 gram CaCl_2 ile başlatılan deneyler NLR analizi ile elde edilmiştir. Hesaplanan reaksiyon hızları 0.5 gram CaCl_2 tuzu ile başlatılan deneylerin sonuçları ile karşılaştırılmıştır. Ön ekspanansiyel faktörler, adsorpsiyon ve desorpsiyon reaksiyonları için sırasıyla $7.06 \cdot 10^{-22} \text{ dk}^{-1}\text{bar}^{-3}$ ve 102 dk^{-1} olarak elde edilmiştir. Ek olarak, görünür aktivasyon enerjileri adsorpsiyon ve desorpsiyon reaksiyonları için sırasıyla $-115600 \text{ J.mol}^{-1}$ ve 23310 J.mol^{-1} olarak elde edilmiştir. Hesaplanan değerler ile deneysel sonuçlar uyum göstermektedir. Dört amonyak ve sekiz amonyak bağlı CaCl_2 tuzları arasında meydana gelen reaksiyonun parametreleri parametreleri 0.5 gram CaCl_2 ile

başlatılan deneylerden hesaplanmıştır. Ön eksponansiyel faktörleri adsorpsiyon ve desorpsiyon reaksiyonları için sırasıyla $2.64 \cdot 10^{-18} \text{ dk}^{-1}\text{bar}^{-3}$ ve 3.44 dk^{-1} olarak elde edilmiştir. Ayrıca, aktivasyon enerjileri adsorpsiyon ve desorpsiyon reaksiyonları için sırasıyla $-88130 \text{ J.mol}^{-1}$ ve 16500 J.mol^{-1} olarak elde edilmiştir. Her iki reaksiyonda da elde edilen negatif görünür aktivasyon enerjileri, reaksiyon mekanizmasındaki karmaşık reaksiyonların varlığını işaret etmektedir.

Kimyasal ısı pompası ve hidrojen depolanması uygulamalarında CaCl_2 pelet formda kullanıldığı için kütle ve ısı transferinin reaksiyon kinetiği ile birleştirildiği teorik bir model oluşturulmuştur. Literatüre katkı olarak hacimsel artış dikkate alınmış ve çalışmada elde edilen tersinir reaksiyon kinetiği kullanılmıştır. Oluşturulan teorik modelde, tersinir reaksiyon kinetiği, ısı ve kütle transferi etkileriyle beraber kullanılmıştır. Simülasyon sonuçlarını karşılaştırabilmek için yassı peletler ile, kinetik parametreleri hesaplaması deneyleri için kullanılan deney düzeneğinde deneyler yapılmıştır. Amonyak basınç düşüşü simülasyon ve deney sonuçları karşılaştırılmıştır. Simülasyon sonuçları ile deney sonuçları iki amonyak ve dört amonyak bağlı CaCl_2 tuzları arasında meydana gelen reaksiyonun için ilk 700 saniyede iyi bir uyum göstermiştir. Sonrasında görülen sapmanın modeldeki sabit efektif difüzyon kabulü kaynaklı olduğu düşünülmektedir. Literatürden elde edilen modelde sabit kabul edilen efektif difüzyon parametresinin, deneyler sırasında değiştiği düşünülmektedir. Buna ek olarak, dört amonyak ve sekiz amonyak bağlı CaCl_2 tuzları arasında meydana gelen reaksiyon sonuçları iyi bir uyum göstermiştir. İlk reaksiyonda görülen sapma, bu reaksiyonda görülmemiştir. Bunun sebebinin, peletin deney sonunda parçalanarak yapısal bütünlüğünü kaybetmesi sebebiyle efektif difüzyon değerinde ciddi bir değişim yaşamamasının, bu değerlerin modelde sabit kabul edilmesi ile uyum göstermesi olduğu çıkarımı yapılmıştır.

Anahtar Kelimeler: Kimyasal Isı Pompası, Hidrojen Depolanması, Reaksiyon Kinetiği, Katı-Gaz Reaksiyonları, $\text{CaCl}_2\text{-NH}_3$

To my whole family...

ACKNOWLEDGMENTS

I would like to express my gratitude to my supervisor, Prof. Dr. Yusuf Uludağ, and co-supervisor, Prof. Dr. Gürkan Karakaş, for their guidance and support throughout my Ph.D. research. I am grateful for the encouragement, patience, and understanding I received from my advisors.

I would also like to thank Berkan Atman, my lab-mate, for his support and motivation. I learned a lot from Alper Sevinç during the demonstration of the experimental setup, and I thank İsa Çağlar, Cemil Araçlı, and Ramazan Küçükdanışman for their assistance during the installation of the experimental setup. I am grateful to my friends from Middle East Technical University, Hande Güneş, Tan Akıncıtürk, Arzu Arslan Bozdağ, Barış Koray Bozdağ, and Işıl Basmaz, for providing me with laughter and support.

I want to extend my thanks to Orhan İnan, Mustafa Çongur, Tuğba Özcan, and Onur Yüksel for their support in the workplace. I am grateful for the conversations I had with Onur about our aspirations, which always served as an inspiration to me.

I would like to thank my family, including my mother Semra Karakaş, brother Emrah Karakaş, and father Bülent Karakaş, my parents-in-love Nurgün Şadiye Helvacı, Enver Helvacı, and brother-in-law Muzaffer Helvacı, for their love and support.

Last but not least, I am grateful to my husband Veysi Helvacı and my son Bartu Helvacı. I could not have completed my Ph.D. without Veysi's support and discussions about my thesis. Bartu was always by my side during my research, and I am motivated to do my best for him in the future. Thank you all for your support throughout this journey.

TABLE OF CONTENTS

ABSTRACT.....	v
ÖZ.....	vii
ACKNOWLEDGMENTS	x
TABLE OF CONTENTS.....	xi
LIST OF TABLES	xiv
LIST OF FIGURES	xv
LIST OF SYMBOLS	xviii
CHAPTERS	
1 INTRODUCTION	1
1.1 Applications of Metal Salt-Ammonia Adsorption/Desorption Systems	1
1.1.1. Chemical Heat Pump	2
1.1.2. Hydrogen Storage Applications	9
1.2 Thermodynamic Constraints and Reaction Mechanism.....	9
1.3 Adsorption/Desorption Phenomena	11
2 LITERATURE REVIEW	15
2.1 Reaction Rate Kinetics	16
2.2 Heat and Mass Transport Phenomena	20
2.3 Structural Change	26
2.4 The Objective of This Study	29
3 METHODOLOGY	33
3.1 Materials and Apparatus.....	33
3.2 Supply Volume Calculation	36

3.3	Reversible Reaction Rate Expression Determination Experiments	
	Procedure with Powder CaCl_2 Metal Salt	37
3.3.1	1 st Adsorption/Desorption Cycle (Ammonia Flush Cycle)	38
3.3.2	Adsorption Reaction Experiment	39
3.3.3	Desorption Reaction Experiment	40
3.3.4	Flow Chart of the Reaction Kinetics Experiments	40
3.4	Heat and Mass Transport Experiments with Pellet CaCl_2 Metal Salt	42
3.4.1	Flow Chart of the Heat and Mass Transfer Experiments	42
3.5	Kinetic Model	44
3.6	Analysis Method	47
3.7	Model Development	48
3.8	Slab Coordinates	51
3.8.1	Heat Transfer Equation.....	51
3.8.2	Mass Transport Equations	54
3.9	Analysis Method	56
3.10	Algorithm of MATLAB	56
4	RESULTS AND DISCUSSION.....	59
4.1	Reaction Rate Kinetics Results and Discussion	59
4.1.1	$\text{CaCl}_2 \cdot (2 \leftrightarrow 4)\text{NH}_3$ Reaction Kinetics Results	59
4.1.2	$\text{CaCl}_2 \cdot (4 \leftrightarrow 8)\text{NH}_3$ Reaction Kinetics Results	69
4.2	Heat and Mass Transport Results and Discussion	84
4.2.1	$\text{CaCl}_2 \cdot (2 \leftrightarrow 4)\text{NH}_3$ Simulation Results	88
4.2.2	$\text{CaCl}_2 \cdot (4 \leftrightarrow 8)\text{NH}_3$ Simulation Results	92
5	CONCLUSION	97
	REFERENCES	101

APPENDICES

A. $\text{CaCl}_2 \cdot (2 \leftrightarrow 4)\text{NH}_3$ Reaction Kinetics Polymath Analysis Results	109
B. $\text{CaCl}_2 \cdot (4 \leftrightarrow 8)\text{NH}_3$ Reaction Kinetics Polymath Analysis Results	114
C. Taylor Expansion	120
D. Discretized Heat Transport Equation	122
E. Discretized Mass Transport Equation	123
F. Volume and Length Calculation of $\text{CaCl}_2 \cdot 2\text{NH}_3$ and $\text{CaCl}_2 \cdot 4\text{NH}_3$ Solid Pellet 124	
G. MATLAB Code	125
CURRICULUM VITAE	145

LIST OF TABLES

TABLES

Table 1. Comparison of Thermal Energy Storage Types (Abedin, 2011).....	4
Table 2. Kinetic parameters used in the Mazet model for $\text{CaCl}_2 \cdot (2 \leftrightarrow 4)\text{NH}_3$ and $\text{CaCl}_2 \cdot (4 \leftrightarrow 8)\text{NH}_3$ reactions (Wang et al., 2008).....	17
Table 3. Kinetic parameters for the reaction of $\text{CaCl}_2 \cdot (2 \leftrightarrow 4)\text{NH}_3$ and $\text{CaCl}_2 \cdot (4 \leftrightarrow 8)\text{NH}_3$ reactions (Oliviera and Wang, 2008).....	18
Table 4. Kinetic parameters for the reaction of $\text{CaCl}_2 \cdot (2 \leftrightarrow 4)\text{NH}_3$ and $\text{CaCl}_2 \cdot (4 \leftrightarrow 8)\text{NH}_3$ reactions (Li et al., 2010).....	19
Table 5. Adsorption and desorption rate constants for 30°C, 45°C, and 55°C when α , β , and γ are 3, 0.1, and 0.3, respectively, for $\text{CaCl}_2 \cdot (2 \leftrightarrow 4)\text{NH}_3$ reaction with initial 0.3 grams of metal salt	62
Table 6. Apparent activation energies and pre-exponential actors of adsorption and desorption rate constants based on the Arrhenius plots and NLR analysis on Polymath and Minitab for $\text{CaCl}_2 \cdot (2 \leftrightarrow 4)\text{NH}_3$ reaction.....	63
Table 7. Adsorption and desorption rate constants for 30°C, 45°C and 55°C when α , β and γ are 3, 0.5 and 0.2, respectively for $\text{CaCl}_2 \cdot (4 \leftrightarrow 8)\text{NH}_3$ reaction with initial 0.5 grams of metal salt.....	73
Table 8. Apparent activation energies and pre-exponential factors of adsorption and desorption rate constants based on the Arrhenius plots and NLR analysis on Polymath and Minitab for $\text{CaCl}_2 \cdot (4 \leftrightarrow 8)\text{NH}_3$ reaction.....	74
Table 9. Material parameters used in the transport simulations	86
Table 10. Simulation parameters for $\text{CaCl}_2 \cdot (2 \leftrightarrow 4)\text{NH}_3$ and $\text{CaCl}_2 \cdot (4 \leftrightarrow 8)\text{NH}_3$	87

LIST OF FIGURES

FIGURES

Figure 1. Illustration of thermochemical energy storage process	3
Figure 2. Schematic illustration of CHP (Li et al., 2016)	7
Figure 3. Clausius-Clapeyron Diagram for mostly used metal salts and liquid-vapor equilibrium line for ammonia (Neveu and Castaing, 1993).....	10
Figure 4. Schematic explanation of adsorption/desorption phenomena (Hill, 1977)	13
Figure 5. Plexiglas reactor a) Side view b) Top view	33
Figure 6. Vacuum Pump	34
Figure 7. Schematic diagram of experimental apparatus	35
Figure 8. Photograph of the demonstrated experimental setup.....	36
Figure 9. Photographs of powder salt a) Before adsorption reaction – in the form of CaCl_2 , b) At the end of the adsorption reaction – in the form of $\text{CaCl}_2 \cdot 8\text{NH}_3$ c) At the end of the desorption reaction – in the form of $\text{CaCl}_2 \cdot 2\text{NH}_3$	39
Figure 10. Flow chart of reaction kinetics experiments.....	41
Figure 11. Flow chart of slab pellet experiments.....	43
Figure 12. Description of grain model	48
Figure 13. Schematic representation of the reactive system.....	50
Figure 14. Slab pellet geometry	51
Figure 15. Salt temperature change inside the salt (open diamonds with round dot line) and degree of conversion for $\text{CaCl}_2 \cdot 4\text{NH}_3$ (closed diamonds) with respect to time for adsorption reaction a) 30°C b) 45°C c) 55°C	61
Figure 16. Arrhenius plots for $\text{CaCl}_2 \cdot (2 \leftrightarrow 4)\text{NH}_3$ reaction a) Adsorption Arrhenius plot b) Desorption Arrhenius plot	63
Figure 17. Adsorption reaction rates versus the molar ratio of $\text{CaCl}_2 \cdot 4\text{NH}_3$ a) 30°C , b) 45°C and c) 55°C ; blue squares represent experimental reaction rates and red diamonds represent calculated reaction rates with initial 0.3 grams of metal salt..	65
Figure 18. Comparison of experimental and calculated adsorption reaction rates with initial 0.3 grams of metal salt. Percentage errors are given in as straight lines: solid	

line: 0 %error, round dotted line 10 % error, square dotted line: 20 % error, dashed line: 30 % error, dashed and dotted line: 45 % error	67
Figure 19. Adsorption reaction rates versus molar ratio of $\text{CaCl}_2 \cdot 4\text{NH}_3$ a) 25°C, b) 45°C; blue squares represent experimental reaction rates, and red diamonds represent calculated reaction rates with initial 0.5 grams of metal salt	68
Figure 20. Salt temperature (open diamonds with round dot line) and degree of conversion for $\text{CaCl}_2 \cdot 8\text{NH}_3$ (closed diamonds) for adsorption reaction at 30°C, 45°C and 55°C, respectively	70
Figure 21. Salt temperature (open diamonds with round dot line) and degree of conversion for $\text{CaCl}_2 \cdot 8\text{NH}_3$ (closed diamonds) for desorption reaction at 30°C, 45°C, and 55°C, respectively	72
Figure 22. Arrhenius plots for $\text{CaCl}_2 \cdot (4 \leftrightarrow 8)\text{NH}_3$ reaction a) Desorption Arrhenius plot b) Adsorption Arrhenius plot	74
Figure 23. Adsorption reaction rates versus the molar ratio of $\text{CaCl}_2 \cdot 8\text{NH}_3$ a) 30°C, b) 45°C, c) 55°C, the blue square represent experimental reaction rates, and red diamonds represent calculated reaction rates with 0.5 grams of initial metal salt ..	76
Figure 24. Desorption reaction rates versus the molar ratio of $\text{CaCl}_2 \cdot 8\text{NH}_3$ a) 30°C, b) 45°C, c) 55°C, the blue square represents experimental reaction rates and the red diamond represents calculated reaction rates with 0.5 grams of initial metal salt ..	78
Figure 25. a) Comparison of experimental and calculated adsorption reaction rates b) Comparison of experimental and calculated desorption reaction rates. Percentage errors are given in as straight lines: solid line: 0 % error, round dotted line 10 % error, square dotted line: 20 % error, dashed line: 30 % error, dashed and dotted line: 45 % error	80
Figure 26. Adsorption reaction rates versus the molar ratio of $\text{CaCl}_2 \cdot 8\text{NH}_3$ a) 30°C, b) 45°C, c) 55°C, the blue square represent experimental reaction rates, and red diamonds represent calculated reaction rates with 0.3 grams of initial metal salt ..	82
Figure 27. Desorption reaction rates versus the molar ratio of $\text{CaCl}_2 \cdot 8\text{NH}_3$ a) 30°C, b) 45°C; the blue squares represent experimental reaction rates, and red diamonds represent calculated reaction rates with 0.3 grams of initial metal salt	83

Figure 28. Pellet representation a) top view of anhydrous CaCl_2 before the $\text{CaCl}_2 \cdot 0 \leftrightarrow 1\text{NH}_3$ reaction b) side view of anhydrous CaCl_2 before the $\text{CaCl}_2 \cdot 0 \leftrightarrow 1\text{NH}_3$ reaction c) top view of $\text{CaCl}_2 \cdot 2\text{NH}_3$ before the $\text{CaCl}_2 \cdot (2 \leftrightarrow 4)\text{NH}_3$ d) top view of $\text{CaCl}_2 \cdot 2\text{NH}_3$ before the $\text{CaCl}_2 \cdot (2 \leftrightarrow 4)\text{NH}_3$	85
Figure 29. Bulk ammonia pressure change with respect to time for $\text{CaCl}_2 \cdot (2 \leftrightarrow 4)\text{NH}_3$ reactions when the initial bulk ammonia pressure is 1.93 bars	88
Figure 30. Local temperature distribution along slab pellet, ξ is the ratio of axial distance to the half of the initial pellet length.....	89
Figure 31. Pressure distribution along the slab pellet, ξ is the ratio of axial distance to the half of the initial pellet length	91
Figure 32. Bulk ammonia pressure change with respect to time for $\text{CaCl}_2 \cdot (4 \leftrightarrow 8)\text{NH}_3$ reactions when the initial bulk ammonia pressure is 2.83 bars	92
Figure 33. Pellet shape a) At the beginning of the $\text{CaCl}_2 \cdot (4 \leftrightarrow 8)\text{NH}_3$ reaction and b) At the end of the $\text{CaCl}_2 \cdot (4 \leftrightarrow 8)\text{NH}_3$ reaction	93
Figure 34. Temperature distribution along slab pellet, ξ is the ratio of axial distance to the half of the initial pellet length.....	94
Figure 35. Pressure distribution along the slab pellet, ξ is the ratio of axial distance to the half of the initial pellet length	96

LIST OF SYMBOLS

A_a	Adsorption reaction pre-exponential factor ($\text{min}^{-1} \text{bar}^{-3}$)
A_d	Desorption reaction pre-exponential factor (min^{-1})
C	Concentration (mol m^{-3})
C_p	Specific heat capacity ($\text{J kg}^{-1} \text{K}^{-1}$)
D_{eff}	Effective Diffusion coefficient ($\text{m}^2 \text{s}^{-1}$)
$D_{\text{eff},0}$	Initial effective diffusion coefficient ($\text{m}^2 \text{s}^{-1}$)
E_{a_a}	Adsorption reaction activation energy (J mol^{-1})
E_{d_a}	Desorption reaction activation energy (J mol^{-1})
g	gravitational force (m s^{-2})
h	convective heat transfer coefficient ($\text{W m}^{-2} \text{K}^{-1}$)
I_0	Reaction source term ($\text{mol m}^{-3} \text{min}^{-1}$)
k_a	Adsorption reaction rate constant (min^{-1})
k_d	Desorption reaction rate constant (min^{-1})
k_{eff}	Effective thermal diffusivity ($\text{m}^2 \text{s}^{-1}$)
L	Length (m)
L_c	Characteristic length (m)
MW	Molecular weight (g mol^{-1})
n	Number of moles (mol)
NA	Mass flux ($\text{mol m}^{-2} \text{s}^{-1}$)
Nu	Nusselt number (-)
P	Pressure (Pa)
P_c	Constraint pressure (Pa)
P_{eq}	Equilibrium pressure (Pa)
Pr	Prandtl number (-)

Q_{ads}, Q_{des}	Adsorption, desorption heat of reaction (J)
Q_c, Q_h	Useful heat, useful cold energy (J)
$Q_{s,bed}$	Reactive bed sensible heat energy (J)
$Q_{s,ev}$	Evaporator sensible heat energy (J)
Q_{in}	Heat consumption during charging phase (J)
r	Radius (m)
R	Gas constant ($J\ mol^{-1}\ K^{-1}$)
Ra	Rayleigh number (-)
t	Time (s)
T	Temperature (K)
T_0	Initial temperature (K)
T_s	Surface temperature (K)
T_∞	Bulk temperature (K)
V	Volume (m^3)
x	Conversion (-)
ΔG	Gibbs free energy ($J\ mol^{-1}$)
ΔH	Enthalpy of reaction ($J\ mol^{-1}$)
ΔS	Entropy of reaction ($J\ mol^{-1}\ K^{-1}$)
α, β, γ	Reaction coefficients (-)
β_e	Thermal expansion (K^{-1})
δ	Stoichiometric coefficient
ε	Porosity (-)
θ	Molar ratio (-)
μ	Dynamic viscosity (Pa s)
ν	Kinematic viscosity ($m^2\ s^{-1}$)
ρ	Density ($kg\ m^{-3}$)

σ Ratio of initial salt mole to initial ammonia mole (-)

Subscript

(0-1) Reaction of ($\text{CaCl}_2 + \text{NH}_3 \leftrightarrow \text{CaCl}_2 \cdot \text{NH}_3$)

(1-2) Reaction of ($\text{CaCl}_2 \cdot \text{NH}_3 + \text{NH}_3 \leftrightarrow \text{CaCl}_2 \cdot 2\text{NH}_3$)

(2-4) Reaction of ($\text{CaCl}_2 \cdot 2\text{NH}_3 + 2\text{NH}_3 \leftrightarrow \text{CaCl}_2 \cdot 4\text{NH}_3$)

(4-8) Reaction of ($\text{CaCl}_2 \cdot 4\text{NH}_3 + 4\text{NH}_3 \leftrightarrow \text{CaCl}_2 \cdot 8\text{NH}_3$)

ads, des Adsorption reaction, desorption reaction

c Cooling

ev Evaporation

h Heating

CHAPTER 1

INTRODUCTION

It is widely recognized that technology is continually improving, and this advancement also drives industrial growth. As a result of these advances in industries and technologies, the energy demand has been increasing globally. Especially petrochemicals and refineries are the main industrial applications using fossil fuels for energy. While fossil fuels are the primary contributors to energy production, they have several drawbacks that cannot be ignored. They are nonrenewable, their availability is limited, and the most significant disadvantage is their contribution to air pollution. They have a significant contribution to the global CO₂ emission that was restricted by Montreal and Kyoto Protocols. Moreover, they release other toxic gases, such as nitrogen dioxide and sulfur dioxide into the atmosphere, contributing to air pollution. Therefore, scientists are trying to find a new approach to this energy demand which is also environmentally friendly.

1.1 Applications of Metal Salt-Ammonia Adsorption/Desorption Systems

One of the ways to turn this disadvantage into some advantages is utilizing the low-temperature waste heat energy by adopting advanced technology such as conventional heat pumps where low-temperature waste heat can be upgraded into high/moderate temperature heat energy. Unfortunately, conventional vapor compression heat pumps typically use refrigerants such as chlorofluorocarbons, hydrofluorochlorocarbons, isobutane, and carbon dioxide. However, these refrigerants are harmful to the environment due to their contribution to greenhouse

gas emissions and ozone layer depletion, leading to the adoption of protocols such as the Kyoto and Montreal agreements, which limit their use (Demir, 2008). Therefore, when these drawbacks of the conventional heat pumps are considered, it can be noted that the technology that will take this advantage one step further is the chemical heat pumps which use the heat of reaction rather than the heat of evaporation as in heat pumps.

Another solution to reduce the need for fossil fuels for energy demand is using hydrogen as an energy carrier. However, the lack of a convenient storage method for hydrogen is the main concern in using hydrogen as an energy carrier. In order to handle the storage and transportation of hydrogen, NH_3 has been proposed as an indirect hydrogen storage material that has a high gravimetric density of hydrogen when it is liquified at 293 K by applying compression pressure higher than 0.85 MPa (Aoki et al., 2014). This high pressure, unfortunately, limits the transportation of hydrogen. Recently, storing NH_3 in the form of metal ammine complexes has been alternatively started to be investigated. For example, 9.1 % of hydrogen can be stored in $\text{MgCl}_2 \cdot 6\text{NH}_3$ in the form of NH_3 . With this method, hydrogen can be stored in metal ammine complexes in solid form, and when it is needed, firstly, ammonia is desorbed from the solid material, and then it is decomposed into its constituents (Hummelshøj et al., 2005).

1.1.1. Chemical Heat Pump

In industrial settings, energy is generated that has a temperature lower than 250°C and is considered waste heat (as stated by Chan et al., 2013). To make this waste heat usable for processes, its quality must be improved since it cannot be used in its current state. One of the ways to utilize energy is the heat pumps. However, after Montreal and Kyoto Protocols, the materials used in this method were restricted due to the harmful effect on the environment (Demir, 2008). Therefore, because of environmental concerns, scientists also gave attention to the usage of environmentally friendly materials. One of the methods for that is chemical heat pumps (CHP). In contrast with conventional heat pumps, CHPs have zero ozone

depletion and global warming potential. Their working temperature range is wider, and also their capacity is high when compared to conventional ones (Li et al., 2009)

The main working principle of chemical heat pumps depends on the ability to store energy in reversible reactions (Abedin, 2011). The thermochemical energy storage process includes three steps: charging, storing, and discharging, as illustrated in Figure 1.

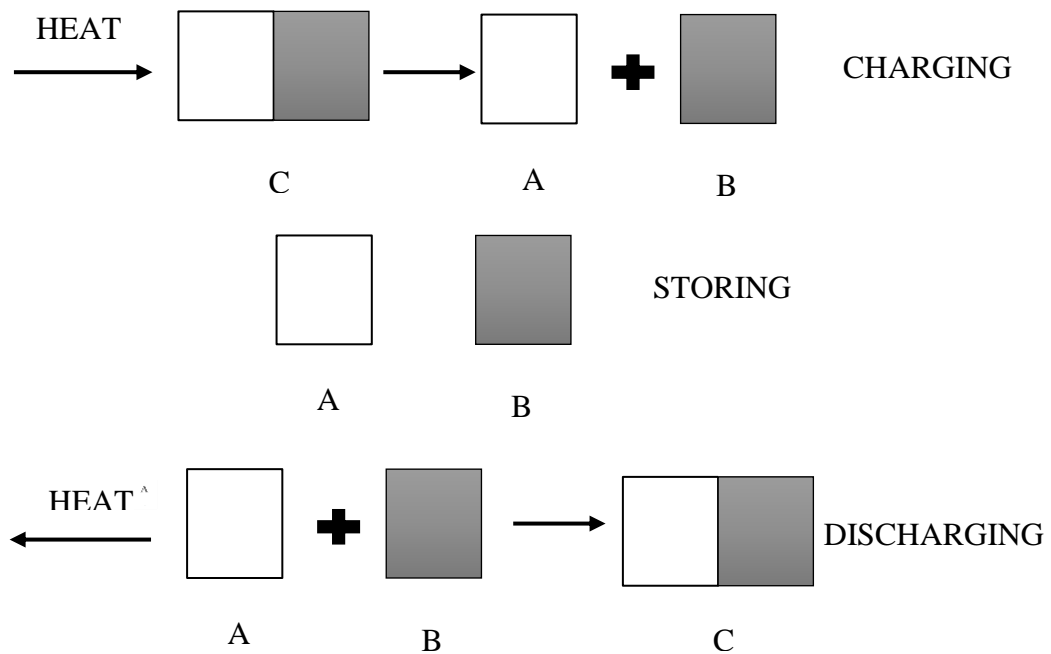


Figure 1. Illustration of thermochemical energy storage process

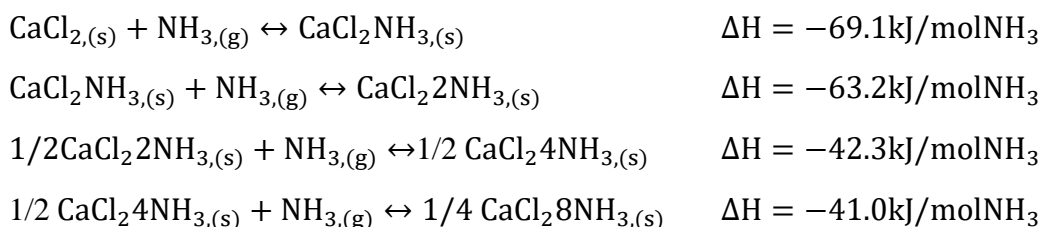
During the charging process, heat is supplied from the surroundings, and component C is separated into components A and B. In the storing process, the supplied energy is stored in components A and B, with little or no energy loss. In the discharging step, components A and B combine to form component C, and the stored heat in components A and B is released. There are three types of thermal energy storage processes: sensible heat storage, latent heat storage, and thermochemical heat storage (Aydın et al., 2015). A comparison of these processes is given in Table 1.

Table 1. Comparison of Thermal Energy Storage Types (Abedin, 2011)

Parameter	Types of Thermal Energy Storage		
	Sensible Thermal Energy Storage	Latent Thermal Energy Storage	Chemical Thermal Energy Storage (Sorption and Thermochemical)
Temperature	Up to: 110°C for water tanks, 50°C for aquifers and ground storage and 400°C for concrete	20-40°C for paraffins and 30-80°C for salt hydrates	20-200°C
Storage Density	Low (0.2 GJ/m ³)	Moderate (0.3-0.5 GJ/m ³)	High (0.5-3 GJ/m ³)
Lifetime	Long	Limited by storage material cycling	Limited by reactant degradation and/or side reactions
Technology Status	Commercially available	Commercially available for specific temperature ranges and materials	Under research

Figure 3 shows the Clausius -Clapeyron diagram of selected metal salts. In this figure, each line is the equilibrium line for the corresponding adsorption reaction system. The reaction rate is equal to zero on this line. Above the equilibrium line, an adsorption reaction occurs, while below the equilibrium line desorption reaction occurs.

The working pairs used in CHPs and hydrogen storage applications should have some requirements based on economical, performance, and safety. When these requirements are considered, CaCl₂ is selected as the metal salt because of its advantages over other metal salts. One of the most important features of this material is that it is non-toxic. Moreover, since CaCl₂ is produced as a side product in industrial applications, it is available and cheap. It is less corrosive and has better thermal and chemical stability. Another important issue is the adsorption capacity, which is the highest among the other metal salts. For example, one mole of CaCl₂ can adsorb eight moles of ammonia. The reaction system between CaCl₂ and NH₃ can be given as follows.



1.3 Adsorption/Desorption Phenomena

Adsorption is the process in which atoms, ions, or molecules adhere to a surface. Adsorption is divided into two categories: physical adsorption and chemical adsorption. In physical adsorption, the molecules are attached to the surface due to intermolecular forces, which are similar to condensation in terms of how they are formed. Therefore, the heat of adsorption is in the range of the latent heat of condensation/evaporation (2 to 21 kJ/mole). Equilibrium can be easily achieved quickly because the energy requirements are low. The forces are weak, so the

activation energy is low (<4 kJ/mole), and the coverage is multilayered. In chemical adsorption, atoms are bonded to the surface due to chemical interactions between the atoms and the surface. The required energy is higher than in physical adsorption and is in the same order as the heat of reaction (21-420 kJ/mole) (Smiths, 1987). Unlike physical adsorption, these systems can be reversible or irreversible, and the activation energy is higher.

The adsorption process involves a series of steps. First, reactants are transferred from the bulk fluid to the solid particle surface (Figure 4/1. Mass transfer through external boundary layer). When the reactant molecules come into contact with the solid particles, molecular diffusion occurs, and the reactant gases move from the external surface to the interior void/pore structure (Figure 4/2. Diffusion into pores). A chemisorption reaction occurs on the pore surface (Figure 4//3. Chemisorption). After the reaction, the gaseous products are desorbed from the solid surface (Figure 4//4-5. Reaction and desorption). Then, the gaseous products diffuse through the interior void/pore to the external surface of the particle (Figure 4/6. Diffusion of products out of pores). Finally, the product gases are transferred from the external surface of the solid particles to the bulk fluid (Figure 4/Mass transfer back to bulk fluid).

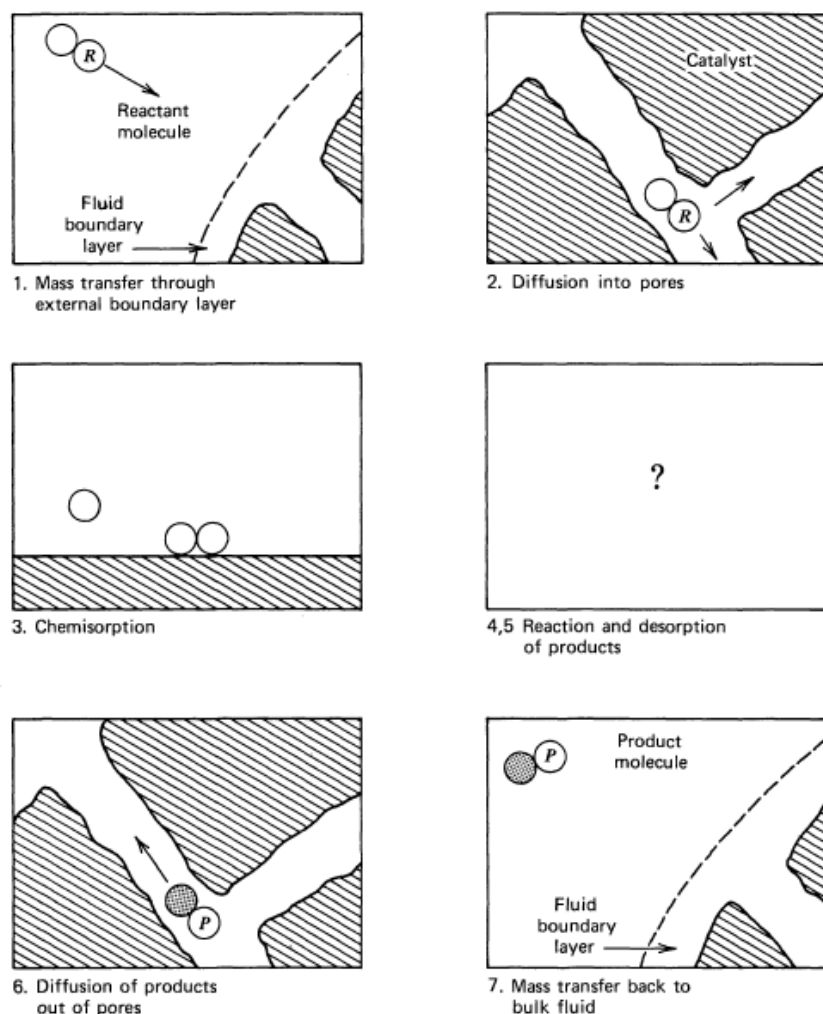


Figure 4. Schematic explanation of adsorption/desorption phenomena (Hill, 1977)

When the reactive system of ammonia-metal salt is considered, the reactant molecule is the ammonia, while the solid surface belongs to the metal salt. During the adsorption reaction of ammonia to the metal salt, steps 1, 2, 3, 4, and 5 in Figure 4 take place consecutively, and at the end of the adsorption reaction, the solid ammoniated metal salt is obtained. On the other hand, during the desorption reaction of ammonia from the metal salt, steps 4, 5, 6, and 7 are followed consecutively in Figure 4.

CHAPTER 2

LITERATURE REVIEW

Despite being widely studied since 1992, the first study on chemical heat pumps conducted by Faraday in 1823. He ammoniated silver chloride in one leg of a sealed bent glass tube, and when heated, the tube produced ammonia gas. In the other leg, he condensed the ammonia gas to obtain liquid ammonia (Critoph, 2012). During his research, Faraday concluded that heat is produced when chloride adsorbs ammonia. He recorded his observations as follows:

“When the chloride of silver is allowed to cool, the ammonia immediately returns to it, combining with it, and producing the original compound. During this action a curious combination of effects takes place: as the chloride absorbs the ammonia, heat is produced, the temperature rising up to nearly 100°C, whilst a few inches.” (Faraday, 1823)

In the years following Faraday's initial study, many researchers continued to investigate chemical heat pumps. In 1915, Dunsford studied an ammonia sorption system using ammonium nitrate as an adsorbent, with a focus on marine applications. The goal of this study was to reduce the agglomeration effect in the system, which was achieved by spreading the adsorbent as a thin layer on a corrugated surface (Dunsford, 1915). In 1925, the combination of sulfur dioxide and silica gel was used in railway carriages as an air conditioner in the United States, and this system was patented in 1929 by Hulse and Miller (Hulse, 1929; Miller, 1929). Prior to 1980, sorption heat pumps were not widely studied, but since then, there has been a significant increase in research on this topic worldwide (Critoph, 2012). Today,

researchers are working to improve the system in order to expand its potential applications, with a focus on achieving continuous cooling and heating, high COP and coefficient of system performance values, and operation with lower temperature energy sources (Demir et al., 2008).

2.1 Reaction Rate Kinetics

The development of an appropriate reaction kinetics expression is critical to predict the system design and scaling. Many studies have been done on this topic, and many reaction kinetics expressions have been suggested for different metal salts-ammonia systems. The common point of all, the reaction rate term was expressed as the multiplication of the reaction progression term and rate constant term. The rate constant term covers the effect of both the Arrhenius term and the thermodynamic equilibrium drop term. The latter term related the constraint pressure and/or temperature and the equilibrium pressure and/or temperature and was suggested in various forms (Mazet et al., 1991; Han et al., 2000; Neveu et al., 1997; Iwata et al., 2014; Lebrun and Spinner, 1990; Dutour, 2005; Azoumah et al., 2007; Lyakh et al., 2013; Le Pierrès et al., 2007; Le Pierrès et al., 2008; Wang et al., 2010; Mofidi and Udell, 2017). One of the first approaches belongs to Mazet et al., in which the Arrhenius term was assumed to be constant since its contribution was relatively small compared to the thermodynamic equilibrium drop (Mazet et al., 1991). The suggested rate expression is given in Equations 10 and 11 for adsorption and desorption reactions, respectively.

$$\frac{dx}{dt} = k_a(1-x)^\alpha \frac{P_c - P_{eq}(T)}{P_c} \quad 10$$

$$\frac{dx}{dt} = k_d(x)^\gamma \frac{P_c - P_{eq}(T)}{P_c} \quad 11$$

In Equations 10 and 11, k_a and k_d represent the reaction rate constant, and α and γ represent kinetic parameters for adsorption and desorption, respectively and x represented the active vacant site. P_c represented the constraint pressure while the

P_{eq} represented the equilibrium pressure with respect to the operating temperature. The Mazet model was used for $\text{CaCl}_2 - \text{NH}_3$ reactive system by Wang et al. for chemical heat pump application (Wang et al., 2008). They studied the performance of the system when two reactive salts, CaCl_2 and MnCl_2 , were used in the chemical heat pump. They mainly focused on the occurrence of the multistep reactions of $\text{CaCl}_2 \cdot (2 \leftrightarrow 4)\text{NH}_3$ and $\text{CaCl}_2 \cdot (4 \leftrightarrow 8)\text{NH}_3$. Metal salt impregnated into the expanded graphite was used in the experiments to enhance thermal conductivity and permeability. This way, the pressure inside the salt matrix and conversion was assumed to be uniform. Three reactors were used; two for CaCl_2 and one for MnCl_2 . Based on the operating conditions, $\text{MnCl}_2 \cdot 6\text{NH}_3$ desorbed ammonia, which was adsorbed by the $\text{CaCl}_2 \cdot 2\text{NH}_3$ or $\text{CaCl}_2 \cdot 4\text{NH}_3$ matrices. It was noted that at high pressure and temperature, both reactions occurred simultaneously. However, according to the equilibrium pressure, operating temperatures had a significant effect on which reaction takes place. The obtained kinetic parameters are given in Table 2.

Table 2. Kinetic parameters used in the Mazet model for $\text{CaCl}_2 \cdot (2 \leftrightarrow 4)\text{NH}_3$ and $\text{CaCl}_2 \cdot (4 \leftrightarrow 8)\text{NH}_3$ reactions (Wang et al., 2008)

Reaction	k_a (s ⁻¹)	α (-)	k_d (s ⁻¹)	γ (-)
$\text{CaCl}_2 \cdot (2 \leftrightarrow 4)\text{NH}_3$	0.0287	1.780	0.0045	0.468
$\text{CaCl}_2 \cdot (4 \leftrightarrow 8)\text{NH}_3$	0.0125	2.104	0.0195	1.005

Another study by the same research group was conducted using modified reaction rate expression (Oliveira and Wang, 2008). The expanded graphite-metal salt matrix was used in the experiments. The theoretical approach considered both pressure and temperature equilibrium drop is given in Equations 12 and 13.

$$\frac{dx_{24}}{dt} = k_a (1 - x_{(2-4)})^\alpha \left(\frac{P\varepsilon}{RT\rho_{SB}} \right)^n \ln \left(\frac{P}{P_{eq,(2-4)}} \right) \left(\frac{1}{T} - \frac{1}{T_{eq,(2-4)}} \right) \quad 12$$

$$\frac{dx_{48}}{dt} = k_d (x_{(2-4)} - x_{(4-8)})^\alpha \left(\frac{P\varepsilon}{RT\rho_{SB}} \right)^n \ln \left(\frac{P}{P_{eq,(4-8)}} \right) \left(\frac{1}{T} - \frac{1}{T_{eq,(4-8)}} \right) \quad 13$$

Here, additionally, n term was added as an exponent factor in the pressure equilibrium drop term. Conversion for the $\text{CaCl}_2 \cdot (2 \leftrightarrow 4)\text{NH}_3$ and $\text{CaCl}_2 \cdot (4 \leftrightarrow 8)\text{NH}_3$ reactions are defined as $x_{(2-4)}$ and $x_{(4-8)}$. Moreover, ε represented porosity in the reactant and ρ_{SB} was defined as the molar density of the metal salt in the bulk reactant. Experiments were conducted at a higher pressure than the equilibrium pressure at the operating temperature. Accordingly, both reactions occurred simultaneously. Still, the primary assumption is that the reaction of $\text{CaCl}_2 \cdot (4 \leftrightarrow 8)\text{NH}_3$ started after the production of $\text{CaCl}_2 \cdot 4\text{NH}_3$. Therefore, for the $\text{CaCl}_2 \cdot (4 \leftrightarrow 8)\text{NH}_3$ reaction. The kinetic coefficients reported in their study are given in Table 3.

Table 3. Kinetic parameters for the reaction of $\text{CaCl}_2 \cdot (2 \leftrightarrow 4)\text{NH}_3$ and $\text{CaCl}_2 \cdot (4 \leftrightarrow 8)\text{NH}_3$ reactions (Oliviera and Wang, 2008)

Reaction	k_a (s^{-1})	α (-)	β (-)
$\text{CaCl}_2 \cdot (2 \leftrightarrow 4)\text{NH}_3$	$1.200 \cdot 10^5$	2	2
$\text{CaCl}_2 \cdot (4 \leftrightarrow 8)\text{NH}_3$	$1.025 \cdot 10^4$	1	1

In the previous studies, the pressure of the salt matrix was kept constant, and adsorption/desorption reactions were initiated by the temperature difference. Li et al. carried out iso-volumetric experiments, where the reactions of $\text{CaCl}_2 \cdot (2 \leftrightarrow 4)\text{NH}_3$ and $\text{CaCl}_2 \cdot (4 \leftrightarrow 8)\text{NH}_3$ did not occur simultaneously. Also, they suggested temperature-dependent reaction rate kinetics with pre-exponential terms and activation energies, given in Equations 14 and 15.

$$\frac{dx_{24}}{dt} = (1 - x_{2-4})^\alpha A_{a(2-4)} \exp \left(\frac{Ea_{a(2-4)}}{RT} \right) \cdot \left| \frac{P_c - P_{eq}(T)}{P_c} \right| \cdot \left(\frac{T - 273}{T_c - 273} \right)^\gamma \quad 14$$

$$\frac{dx_{48}}{dt} = (1 - x_{4-8})^\alpha A_{d(4-8)} \exp\left(\frac{Ea_{a(4-8)}}{RT}\right) \cdot \left|\frac{P_c - P_{eq}(T)}{P_c}\right| \cdot \left(\frac{T - 273}{T_c - 273}\right)^\gamma \quad 15$$

Different from the previous models, temperature drop had an exponent factor represented as γ . Instead of a regression method, the reaction expression parameters were evaluated by the integration method. Table 4 shows the kinetic parameters with the pre-exponential term and activation energies.

Table 4. Kinetic parameters for the reaction of $\text{CaCl}_2 \cdot (2 \leftrightarrow 4)\text{NH}_3$ and $\text{CaCl}_2 \cdot (4 \leftrightarrow 8)\text{NH}_3$ reactions (Li et al., 2010)

Parameters				
Reaction	α (-)	A_a (s^{-1})	Ea_a ($\frac{\text{J}}{\text{mol}}$)	γ (-)
$\text{CaCl}_2 \cdot (2 \leftrightarrow 4)\text{NH}_3$ Adsorption	2	$2.04 \cdot 10^{-3}$	1383.24	4
$\text{CaCl}_2 \cdot (4 \leftrightarrow 8)\text{NH}_3$ Adsorption	6	$1.75 \cdot 10^{-2}$	3316.95	-1.2
Reaction	α (-)	A_d (s^{-1})	Ea_d ($\frac{\text{J}}{\text{mol}}$)	γ (-)
$\text{CaCl}_2 \cdot (2 \leftrightarrow 4)\text{NH}_3$ Desorption	2	$0.5 \cdot 10^{-3}$	2385	4
$\text{CaCl}_2 \cdot (4 \leftrightarrow 8)\text{NH}_3$ Desorption	6	$2.75 \cdot 10^{-3}$	1174.55	1.2

In all studies, the adsorption and desorption reaction rates were expressed individually and dependent on the equilibrium drop term. The equilibrium drop term was suggested as pressure equilibrium drop or temperature equilibrium drop or a combination of pressure and temperature equilibrium drop terms.

2.2 Heat and Mass Transport Phenomena

Modeling solid/gas reactions is important in various industries, as it allows for predicting temperature, pressure, and conversion within the solid undergoing a reaction. Developing a complete model is particularly useful for dangerous, expensive, and time-consuming systems, as it allows for optimizing system parameters. There are several different methods for modeling solid-gas reactions, including the sharp interface model (also known as the shrinking core model), the volume reaction model, the pore model, the network model, and the particle/pellet model (Hastaoglu and Abba, 1996). The shrinking core model is widely used for modeling the reaction between ammonia and metal salts.

In 1991, Mazet, Amouroux, and Spinner studied the reaction mechanism between $\text{CaCl}_2 \cdot 6\text{CH}_3\text{NH}_2 - \text{CaCl}_2 \cdot 4\text{CH}_3\text{NH}_2$ (Reaction-1) and $\text{CaCl}_2 \cdot 4\text{CH}_3\text{NH}_2 - \text{CaCl}_2 \cdot 2\text{CH}_3\text{NH}_2$ (Reaction-2) in order to utilize the heat of reaction for chemical heat pump applications. In their experimental study, the researchers used a cylindrical chamber filled with anhydrous salt to evaluate global advancements. The chamber was heated from the outer surface and supplied with reactant gas through the hollow center. A highly porous pellet was used, and the pressure was assumed to be uniform throughout the pellet, which was confirmed by the experimental results (the difference was less than 0.1 bar for a constraint pressure of 2.8 bar). The reaction was initiated at a temperature and pressure that differed from thermodynamic equilibrium values. Because the reaction was endothermic, it absorbed the sensible heat of the medium as it progressed. This caused the temperature to drop rapidly at the beginning of the reaction. As time passed, the temperature at each point in the cylindrical reactor increased due to the heat transfer fluid and eventually reached the constraint temperature. The experimental measurements showed a strong temperature difference that could be modeled mathematically. In some cases, the constraint temperature and pressure for both reactions were the same, so the researchers treated the reactions as occurring simultaneously and modified the reaction rate equations. They assumed that the Arrhenius term in the reaction rate

constant was constant because the reaction was mainly influenced by thermodynamic conditions. This allowed them to evaluate the parameters experimentally. According to their simulations, the two reactions occurred simultaneously near the outer wall of the cylindrical reactor due to the heat transfer fluid. However, near the hollow center (away from the heat exchanger fluid), the activity of each reaction could be distinguished easily. The local advancements of the two reactions were localized in a narrow front that moved from the outer surface to the center of the reactor with the heat transfer front, as indicated by the temperature gradient. A negative deviation from thermodynamic conditions resulted in a decrease in thermal power, which could be recovered from the system. However, the assumption of a constant Arrhenius term introduced some errors due to its high temperature dependency. In addition, it is important to determine the relationship between the constraint conditions and changes in parameters (Mazet et al., 1991).

In 1992, Goetz and Marty investigated $\text{MnCl}_2\text{-NH}_3$ reactive system both experimentally and theoretically. In the study, they used the grain-pellet model in which grain gave information about the local conversion, temperature, and pressure while pellet gave global information. Their assumptions behind the model were as follows:

- There was a sharp interface between the reactant and the product. Gas diffused through the product and reacted on the reactant surface (interface)
- As the reaction proceeded, the interface moved toward the center of the grain
- The size of the grains was uniform
- The number of grains was constant
- The porosity of the grain and the pore diameter were constant

Because of the difference in the molar volumes of the reactants and the products, structural changes happen. In the study, an increase in the molar volume during the adsorption reaction was attributed to the grains' expansion, and a decrease in the molar volume during the desorption reaction was attributed to the contraction of the grains. At the grain level, the temperature was assumed to be uniform. Their

theoretical study at the grain level was demonstrated for mass transfer, and at the pellet level was demonstrated for heat transfer. According to their simulation results, they noted that the reaction rate was strongly dependent on equilibrium temperature and equilibrium pressure drop. Also, they concluded that the global advancement of the medium was related to the progress of the reaction zone which was controlled by the conductive heat transfer (Goetz and Marty, 1992).

In 1995, Lu and co-workers studied $\text{MnCl}_2\text{-NH}_3$ reactive system in which an unreacted shrinking core model was applied. At the grain level, only mass transfer was considered, while heat and mass transfer were considered at the pellet level. As the reaction proceeded, due to the increase in the molar volume of products, grain diameter increased while core diameter decreased because of the consumption of the reactants. At the grain level, porosity was assumed to be constant, grains were assumed to be in a uniform size and shape, and they were assumed spherical. At the pellet level, heat and mass transfer were considered only in the radial direction for a cylindrical pellet shape. Their simulation results noted that both “heat front” and “mass front” were obtained during transformation. Also, it was emphasized that permeability became an important parameter for global advancement when the constraint pressure was lower than 1 bar. But, as pressure increased up to 5 bars, the influence of permeability decreased. Moreover, they concluded that when constraint pressure was higher than 4 bars and permeability larger than 10^{-13} m^2 , the model that considered only heat transfer in the pellet level was in agreement. On the other hand, the present model was found to be suitable (Lu et al., 1995).

In 1997, Stitou, Goetz, and Spinner concentrated on developing a simplified model. In order to increase the heat and mass transfer properties of the salt, they used an ENG binder in suitable proportions. In the simplified model following assumptions were made;

- Porosity was sufficiently high to ensure that mass transfer was not a limiting factor within the bed

- Thermal conductivity and heat transfer coefficient were assumed to be constant, and they were not affected by the advancement and temperature
- Heat transfer was assumed to be only in the radial direction
- External heat and mass transfer were assumed to be constant
- Sensible heat consumed or produced by the medium was assumed to be negligible when compared to the effective molar heat capacity of the reactive medium

A simplified model was developed for different reactor geometries and compared with the dynamic model, which considered mass transfer in the grain scale and heat transfer in the pellet scale. Their comparison showed well agreement. Moreover, the simplified model was compared with the experimental results, which also showed well-agreement. Hence, they concluded that the simplified model quickly responded to the pre-dimensioning of thermochemical machines without much effort (Stitou et al., 1997).

Even though many studies were concentrated on heat transfer at the macroscopic level, Han et al. studied coupled heat and mass transfer at the pellet level. The MnCl_2 -Graphite complex was used in this study to increase the system's thermal conductivity and permeability. These thermo-physical properties were experimentally calculated, and it was observed that both properties increased as the weight fraction (f_g) of graphite increased. For the same bulk density (ρ_b) (100 kg/m^3), thermal conductivity increased from 11.7 W/m.K to 14.8 W/m.K , and permeability increased from $8 \cdot 10^{-14} \text{ m}^2$ to $2.5 \cdot 10^{-13} \text{ m}^2$ for f_g from 30% to 50%, respectively. On the other hand, the relation for permeability was vice versa for the bulk density (ρ_b). For the same f_g (50%), thermal conductivity increased from 14.8 W/m.K to 25.6 W/m.K , and permeability decreased from $2.5 \cdot 10^{-13} \text{ m}^2$ to $8.1 \cdot 10^{-15} \text{ m}^2$ for ρ_b from 100 kg/m^3 to 250 kg/m^3 , respectively. Also, it was observed that there was not a huge change either in thermal conductivity or permeability when the ammoniated moles changed. In this study, both effects of ρ_b and f_g were studied. According to their results, no heat front was observed, meaning that heat transfer was not a limiting

factor for this system. Yet, as ρ_b increased, the mass front became more dominant, especially at low-pressure values. Although increasing the pressure could have solved this problem, it was not preferred for practical applications since it would also lower the COP. Lastly, a decrease in f_g led to a decrease in global conversion because the lower the weight fraction of graphite, the lower the thermal conductivity and permeability (Han et al., 2000).

In the same year, a study was demonstrated to give insight into the diameter of the pellet used in refrigeration operation, done by Enibe and Iloeje. Different from Mazet et al., they assumed that reactions occur in order means that the succeeding reaction did not start before the proceeding reaction ended. Their model was developed according to the “volume reaction model”. Moreover, similar to other studies, the pellet's size, shape, and thermo-physical properties were assumed to be constant to simplify the model. Since the main concern was the decision of the diameter of the pellet used in refrigeration operation, pellets with different diameters were selected. The concentration of adsorbed ammonia and the pellet temperature at the core and the surface were evaluated and compared. It was observed that in a very short time, the pellet mean free gas pressure became almost 95% of external ammonia gas pressure, and no deviation showed mass transfer restriction was negligible. Also, the temperature of the pellet immediately increased and then came into equilibrium in a longer time which was attributed to the faster reaction rate at the beginning of the reaction. For the pellets having a smaller diameter, the difference in concentration of adsorbed ammonia and temperature of the pellet at the core and the surface is smaller when compared to pellets having a larger diameter. Hence, they concluded that a lower pellet size should be selected in order to maintain adsorbent stability (Enibe and Iloeje, 2000).

In 2004, Huang and co-workers investigated the SrCl_2 -IMPEX block in terms of heat transfer coupled with global advancement. The experiments were conducted for a cylindrical annular shape of SrCl_2 -IMPEX block in which ammonia gas was diffused through the annulus while the block was heated by external coils from the external wall of the block. In the theoretical model, the assumptions were;

- The mass transfer was assumed to be negligible
- Heat conduction in the axial direction was assumed to be negligible
- Due to the low gas flow rate during adsorption and desorption reactions, convective heat transfer was assumed to be negligible.
- The thermal capacity of the bed and effective thermal conductivity were assumed to be functions of temperature

In this study, the adsorption and desorption reaction rate kinetics were given separately for adsorption and desorption. Also, the heat balance equation is expressed individually for both reactions. After determining radial temperature values experimentally, kinetic equations are solved for local conversion, enabling them to calculate the global conversion. After that, using the optimization toolbox of MATLAB, kinetic coefficients for both adsorption and desorption reactions were calculated. These obtained parameters were used in the heat transfer equation to investigate significant parameters. Among these parameters, while the heat capacity of the medium effect seemed not so important, the effective thermal conductivity of the bed and convective heat transfer coefficient effects were significant. Hence, keeping the constant value of heat capacity, several experimental data measured at different constraint temperatures and pressures allowed them to calculate effective thermal conductivity and convective heat transfer coefficient. Lastly, theoretical results with obtained values were compared with the experimental results, and concluded that they were in good agreement (Huang et al., 2004).

In 2017, Mofidi and Udell studied the $\text{MgCl}_2\text{-NH}_3$ working pair for the purpose of thermochemical batteries, both theoretical and experimental. Although they used different types of metal salt, they used the kinetics proposed for $\text{MgCl}_2\text{-NH}_3$ by Han et al. (Mofidi and Udell, 2017). A cylindrical reactor consisting of $\text{MgCl}_2 \cdot 2\text{NH}_3$ + graphite was used. It was heated from the center by a cartridge, and cool air was supplied from the external annulus. Ammonia was supplied from an ammonia storage tank by a mass flow controller. For the temperature controller, 33 thermocouples were placed at different axial and radial positions. Unlike other

studied models, the governing equations were expanded into three dimensions for the theoretical model. They observed that heat transfer was the limiting factor, especially for the system having high permeability both theoretically and experimentally. Hence, an increase in the system's thermal conductivity would lead to an increase in reaction rate. Yet, theoretical and experimental studies were not in good agreement, which was attributed to the missing reaction rate kinetics parameters.

In two years, Mofidi and Udell extended their research for the scale-up of thermochemical batteries. There were two possible methods: multi-cell reactors or scale-up single-cell reactors. When multi-cell reactors were used, it was observed that although at a high flow rate of ammonia, the adsorption rate was uniform in each cell, it became divergent at a low flow rate of ammonia. This divergence was attributed to two reasons; permeability difference in each cell and temperature dependence of reaction rate. In both situations, scale-up a single cell seemed to be a better way. Before the experiments, it was suggested that scaling up a single cell could cause a decrease in mass transfer limitation by creating or adding additional space for the gas flow passages. After the experiments, it was observed that as reaction occurred, grains expanded, yielding a decrease in permeability and hence mass transfer limitation. However, it was possible to control the adsorption reaction rate, duration of the adsorption process, and temperature of the reactor by controlling the mass flow rate of ammonia (Mofidi, 2019).

2.3 Structural Change

In many solid/gas reaction systems, the structure of the solid changes due to the reaction and temperature gradient. These changes can include shrinkage or closure, pore volume change, swelling, softening, disintegration, agglomeration, and cracking of particles. In metal salts/ammonia reactive systems, the most common changes observed are agglomeration, swelling, and disintegration (Wang et al., 2004). Additionally, it is known that the molar volume of the products is almost

twice that of the reactants, resulting in an increase in volume in the final product. These structural changes can be investigated using BET and XRD measurements and also visually.

In 2004, Wang and colleagues studied the $\text{CaCl}_2\text{-NH}_3$ adsorption/desorption system (Wang et al., 2004). They chose CaCl_2 as the salt because it had a high ammonia adsorption capacity and a fast sorption rate. However, these systems have a significant drawback: during adsorption/desorption, swelling, disintegration, and agglomeration can occur, which strongly affects the system's performance. As agglomeration depends on volume and expansion space, the researchers prepared four samples with different adsorbent thicknesses. The experiments showed that the performance of 2 mm and 3 mm thick adsorbents was similar, as was the performance of 5 mm and 4 mm thick adsorbents. It was also observed that the 2- and 3-mm thick adsorbents degenerated and their performance decreased from 7.15 mole/mole to 5.86 mole/mol. In contrast, the 4- and 5-mm thick adsorbents were not affected by agglomeration and their performance remained stable. However, the performance of the 5 mm thick adsorbent was not as good as that of the 4 mm thick adsorbent due to a limited expansion space, which affected mass transfer. Additionally, 2 mm and 4 mm thick adsorbents were compared after the adsorption of ammonia. Agglomeration was observed in 4 mm thick adsorbent, while it was not observed for 2 mm thick adsorbent. Hence, it was concluded that agglomeration had a crucial relationship with the system's performance. Furthermore, this study concluded that the working pair characteristics had an impact on adsorption/desorption performances. When they repeated the cycles, they observed an approximately 22% decrease in the adsorption performance at the seventh cycle. But they did not do any characterization and therefore it was reported that the agglomeration was the only reason for this decrease. Still, to better understand the system performance as the cycle number increases, the structure of the salt after desorption should be investigated.

In 2005, Christensen and co-workers examined the ammonia adsorption/desorption system of MgCl_2 salt for hydrogen storage since $\text{Mg}(\text{NH}_3)_6\text{Cl}_2$ can store 9.1%

hydrogen as ammonia. They investigated the desorption rate with respect to temperature and repeated the cycles two times. Based on their experiments, desorption started at 350 K, 500 K, and 550 K. After the desorption of ammonia, salt was again saturated with ammonia and the desorption processes repeated. It was seen that it was well matched with the first experiments, so it was concluded that these processes were completely reversible. Moreover, it was observed that MgCl_2 developed its own pore structure during this process. The pellet like salt remained its shape but became very porous. BET measurements showed that after desorption, the surface area became $32\text{m}^2\text{g}^{-1}$, which showed that a Nano-porous structure was formed. However, these measurements were done only for two cycles (Christensen et al., 2005).

In 2005, Hummelshøj and co-workers investigated the reason for the generation of the nano-porous structure of MgCl_2 during ammonia adsorption/desorption system for hydrogen storage applications. They concluded that the formation a nano-porous structure facilitated the transport of ammonia. They calculated the pore size distribution for a different amount of ammonia desorbed. It was concluded that as the amount of desorbed ammonia increased, the average pore diameter size increased from 2-3 nm to almost 20 nm. That's why the kinetics of fine powder particles was similar to that of completely compact samples (Hummelshøj et al., 2005).

In 2006, Elmøe and co-workers used the high ammonia storage capacity of metal chloride salts for NO_x reduction with the SCR method. For the experiments, they used both powder and compacted metal ammine salts. The powder salt's packing density was 331 kg/m^3 , while the compact packing density was 1219 kg/m^3 . But, when the salt was compacted, the porosity decreased. However, the formation of a nano-porous structure during the desorption of ammonia satisfied the necessary porous structure for utilizing the mass transfer (Elmøe et al., 2006).

In 2007, Jacobsen and co-workers investigated the thermal decomposition of $\text{Mg}(\text{NH}_3)_6\text{Cl}_2$ using small-angle X-ray scattering (SAXS). This method provided information about the material's structure by measuring the intensity of scattered

light and the variation with scattering angle. For the experimental studies, the capillary tube was placed in the sample cell and filled with He at 2 bars. The sample was heated to 350°C in steps of 20°C/12 min. Then 5 minutes was waited for the stabilization of the system. Guinier's regime proved the growth of crystallite and pores. Also, since there was no additional structure to the system, the second Guinier regime was supposed to be due to scattering from a porous structure. Based on their studies, they observed the development of pore structure at a temperature above 249°C (Jacobsen et al., 2007).

In 2015, Aoki and co-workers studied how kinetics change with respect to the change in the structure of metal ammine complexes. For that purpose, they compared the kinetics of the reaction with and without NH₃ treatment and investigated the effect of ball milling since it also changed the crystal structure of the salt. They reported that NH₃ treatment improved the kinetics of this reaction due to preserving the apparent volume after ammonia desorption. They also concluded that changing the structure properties by ball milling decreased the activation barrier for this reaction system (Aoki et al., 2015).

2.4 The Objective of This Study

Suggested reaction rate expressions in the literature given in the Section 2.1 reveals that, adsorption and desorption reactions were defined separately for these systems. The operating reaction conditions were decided according to the equilibrium pressures and temperatures for adsorption and desorption reactions. It was noted that the reactions occurred at non-equilibrium conditions meaning that at a selected operating temperature, when the operating pressure was higher than the equilibrium pressure, adsorption reaction takes place and when it is lower than the equilibrium pressure, desorption reaction occurs. When the operating and the equilibrium pressures are equal, then the adsorption or desorption reaction rate is zero according to the Equations 10 - 15. However, according to the Langmuir-Hinshelwood model, at the equilibrium conditions, the reaction rate of adsorption and desorption are equal

to each other and the net reaction rate becomes equal to zero. Expressing more realistic reaction rate is very significant in the calculations of the efficiency of the CHPs. As mentioned previously, the efficiency of a CHP is defined as COP which relates the useful heat/cold production and heat input to the system. In the CHPs, the heat input and useful heat recovery includes the heat of reaction which is related to the reaction rate as given in Equation 6. However, the reaction rate expressions in the literature do not capture the reactive system's reversibility. Therefore, in order to obtain a reaction rate expression which is more in line with reality, in the first part of this study, reaction kinetics of the $\text{CaCl}_2\text{-NH}_3$ reactive system was examined and experimental setup was demonstrated where the reactions are conducted at constant temperature.

For the CHP applications, generally packed bed reactors with metal salt impregnated into graphite or carbon are used in order to increase the thermal conductivity and permeability of the system (Mofidi and Udell, 2019, Mofidi and Udell, 2017, Han et al., 2000, Enibe and Iloje, 2000). Another approach may be using packed bed reactors with pellet shape metal salts. Therefore, understanding the system is very crucial. However, some critical issues related to the heat and mass transfer of ammonia through the pellet in the adsorber/desorber reactor limit the efficiency of these systems. During the ammonia adsorption reaction, the structural change caused by the difference in the molar volumes of reactants and products may lead to heat and mass transfer limitations because of decreasing porosity and permeability. The structural change during the ammonia adsorption reaction is also very significant in the hydrogen storage application because in order to increase the sorption capacities of ammonia, pellet shape metal salts are used (Elmøe et al., 2006, Christensen et al., 2005, Hummelshøj et al., 2005). Therefore, investigating the structural change during the ammonia adsorption is important since it strongly effects the system repeatability and reproducibility. Hence, in the second part of this study, reactive system was studied when CaCl_2 is used in the pellet form experimentally and theoretically. Different from the literature, the obtained reversible reaction kinetics

are aimed to be used in the model. Moreover, the increase in the volume of the pellet was taken into consideration in the model as a contribution to the literature.

Considering the abovementioned reasons, the objectives of this study are as follows:

- Obtaining the reversible reaction rate kinetics for the $\text{CaCl}_2 \cdot (2 \leftrightarrow 4)\text{NH}_3$ and $\text{CaCl}_2 \cdot (4 \leftrightarrow 8)\text{NH}_3$ reactions, accounting for the reversible nature of the reaction.
- Developing a comprehensive and predictive model for $\text{CaCl}_2 \cdot (2 \leftrightarrow 4)\text{NH}_3$ and $\text{CaCl}_2 \cdot (4 \leftrightarrow 8)\text{NH}_3$ reactions when CaCl_2 salt is in pellet form, taking into account heat and mass transfer transport phenomena coupled with the reaction kinetics with the consideration of volume increase.
- Observing the structural change of the salt during the adsorption reaction when the CaCl_2 is in the pellet form experimentally.

4. When valve 2 was opened, nitrogen gas pressure was introduced to the reactor and hence decreased down to P_2 which was the nitrogen gas pressure in the piping volume between valves 4, 2, and 1, including pressure transducer-2, gas cylinder and the reactor. Since the nitrogen gas amount was the same in both cases, the following equation can be written according to the ideal gas law.

$$P_1V_1 = P_2(V_1 + V_3) \quad 16$$

In order to solve Equation 16, another equation was needed, which was obtained by using a known volume material, a non-porous glass ball. The same procedure was followed described above. The pressure of nitrogen gas in the piping volume between valves 4, 2, and 1, including pressure transducer-2 and gas cylinder, was recorded as P_3 . When Valve 2 was opened, the nitrogen gas pressure decreased down to P_4 , which corresponded to the nitrogen gas pressure inside the piping volume between valves 4, 2, and 1, including pressure transducer-2, the gas cylinder, and the reactor. In this case, the reactor contained a small glass ball; hence the volume was written correspondingly as given in Equation 17.

$$P_3V_1 = P_2(V_1 + V_3 - V_b) \quad 17$$

In Equation 17, V_b is the volume of the non-porous glass ball. The solution of these two equations gives the supply volume. Experiments were conducted with different pressure values, and the average of the calculated volumes was used. The same procedure was followed for calculating volume, including pressure transducer-1 and Valve 1.

3.3 Reversible Reaction Rate Expression Determination Experiments Procedure with Powder CaCl_2 Metal Salt

Both volume measurement tests and leak tests were carried out using Nitrogen gas. A fresh sample was introduced to the reactor at the beginning of each temperature

experiment. Before the reaction kinetics experiments, anhydrous CaCl_2 powder was heated and held at 225°C overnight to remove any adsorbed water vapor. Each sample was transferred to the reactor immediately after weighing. Samples were further dried in the reactor by vacuum for at least 30 minutes before the adsorption reaction started. Reaction rates become independent of initial solid particle size, the number of cycles, and the conversion of solids after the first cycle of adsorption/desorption reaction (Diawara, 1986). Therefore, salts were firstly flushed with ammonia at each temperature, and second adsorption/desorption cycle results were taken into consideration in the calculations.

3.3.1 1st Adsorption/Desorption Cycle (Ammonia Flush Cycle)

The entire system was evacuated by vacuum. When the required vacuum was achieved ($<10^{-3}$ mbar), ammonia gas was sent to the small ammonia gas cylinder in the water bath, and Valve V4 is closed. As soon as the valve V2 is opened, the adsorption reaction starts. The adsorption reaction was monitored by the pressure decrease via the pressure transducer. The adsorbed ammonia amount was calculated from the pressure change according to the ideal gas law with the constant volume assumption. When the pure CaCl_2 salt adsorbed 8 moles of ammonia per mole of salt, 1st adsorption reaction was finished, which was followed by the 1st desorption reaction. In this case, the system temperature was kept constant, and pressure was decreased by vacuum. The increase of the pressure monitored the desorption reaction, and the desorbed amount of ammonia was calculated by the same method of 1st adsorption reaction. After 6 moles of ammonia desorbed, 1st adsorption/desorption cycle was finished. Due to very low equilibrium pressures for the reaction of $\text{CaCl}_2 \cdot (0 \leftrightarrow 1)\text{NH}_3$ and $\text{CaCl}_2 \cdot (1 \leftrightarrow 2)\text{NH}_3$ at the working temperatures (25°C , 45°C , 55°C), further desorption reaction did not occur.

At the beginning of the 1st cycle, the salt particles are placed in a movable condition without being compressed, as can be seen in Figure 9-a. At the end of the 1st adsorption reaction, the occupied volume of salt increased and some cracks were

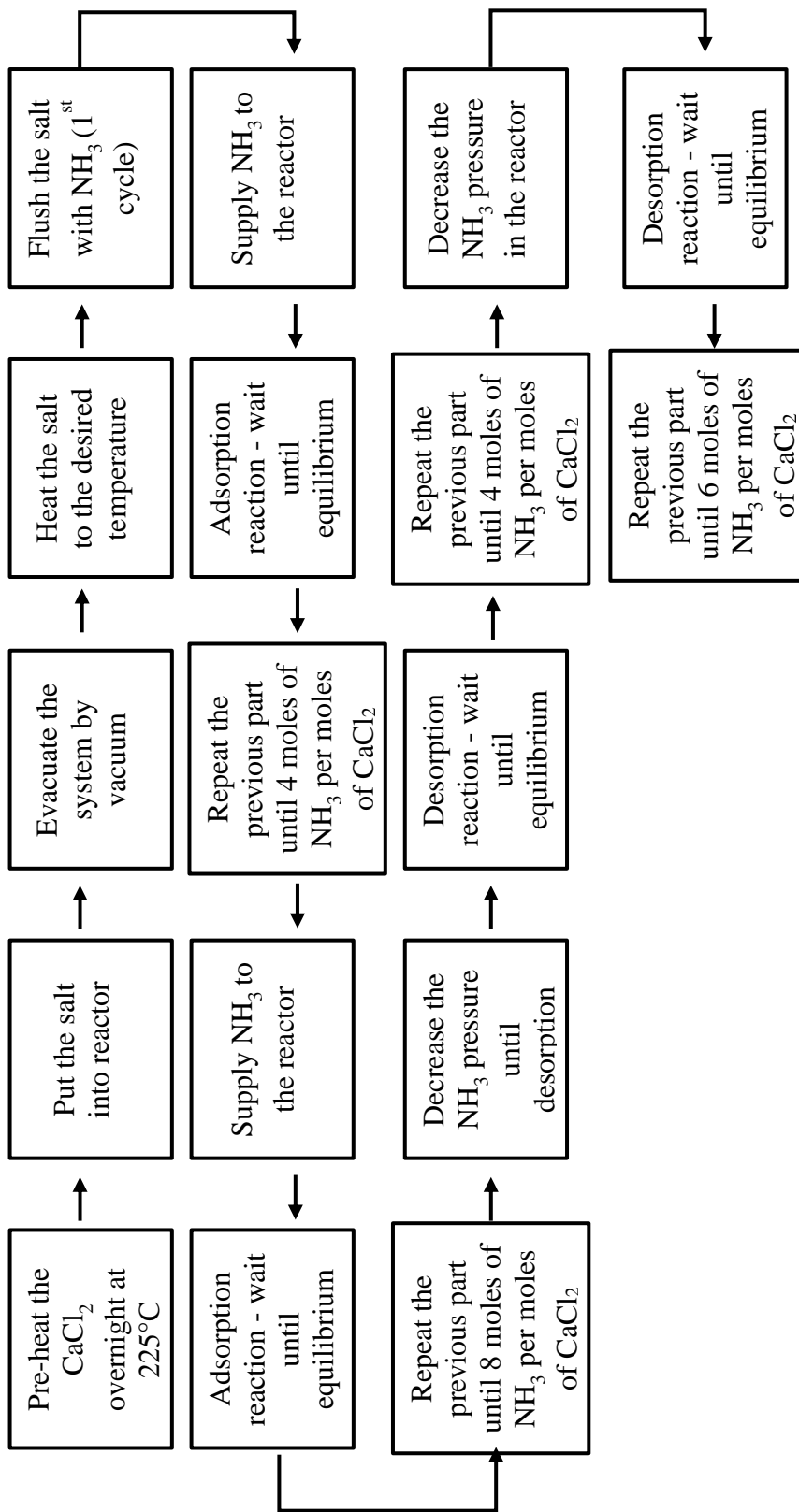


Figure 10. Flow chart of reaction kinetics experiments

3.4 Heat and Mass Transport Experiments with Pellet CaCl₂ Metal Salt

Before making pellets, anhydrous CaCl₂ powder was put into an oven at 225°C and waited overnight. After removing any adsorbed water vapor, pellets were obtained by compression at 60 kN force. Since during this process, pellets might adsorb water vapor from the surroundings, they were also put into an oven at 225°C for additional three days. Just before the experiment, the 0.45 grams of CaCl₂ pellet was put into the reactor immediately. The transport experiment was conducted at 45°C; therefore, the water bath was heated and when the temperature was stabilized, ammonia gas was sent through the reactor and an adsorption reaction was initiated. In the heat and mass transport experiment, the focused reaction was the first adsorption reaction to observe the structure change. When the system reached equilibrium, additional ammonia gas was sent to the reactor and this procedure was followed until 8 moles of ammonia per mole of CaCl₂ was adsorbed totally.

3.4.1 Flow Chart of the Heat and Mass Transfer Experiments

The flow of the heat and mass transfer experiment can be found in Figure 11.

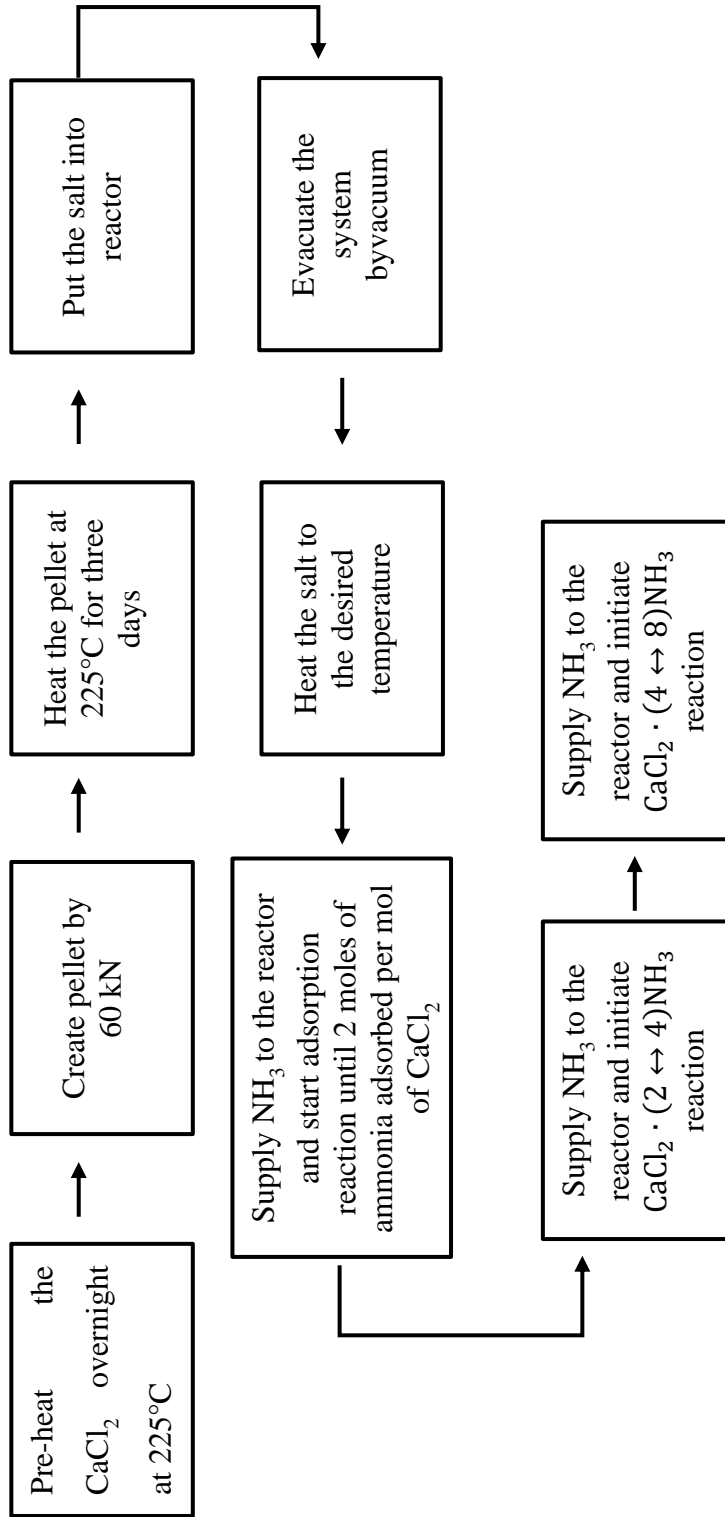


Figure 11. Flow chart of slab pellet experiments

3.5 Kinetic Model

Adsorption and desorption reactions were carried out, and the adsorbed/desorbed amount was calculated by the change of pressure in the volumetric method. Ammonia was assumed to be an ideal gas, and the adsorbed ammonia amount was calculated according to the ideal gas law. The reaction kinetics was expressed based on the change in the molar ratio of $\text{CaCl}_2 \cdot 8\text{NH}_3$ for $\text{CaCl}_2 \cdot (4 \leftrightarrow 8)\text{NH}_3$ reaction and $\text{CaCl}_2 \cdot 4\text{NH}_3$ for $\text{CaCl}_2 \cdot (2 \leftrightarrow 4)\text{NH}_3$ reaction in time that are expressed in Equations 18 and 19.

$$\theta_{\text{CaCl}_2 8\text{NH}_3} = \frac{n_{\text{CaCl}_2 8\text{NH}_3}}{n_{\text{CaCl}_2 8\text{NH}_3} + n_{\text{CaCl}_2 4\text{NH}_3}} \quad 18$$

$$\theta_{\text{CaCl}_2 4\text{NH}_3} = \frac{n_{\text{CaCl}_2 4\text{NH}_3}}{n_{\text{CaCl}_2 2\text{NH}_3} + n_{\text{CaCl}_2 4\text{NH}_3}} \quad 19$$

In Equations 18 and 19, $n_{\text{CaCl}_2 8\text{NH}_3}$, $n_{\text{CaCl}_2 4\text{NH}_3}$ and $n_{\text{CaCl}_2 2\text{NH}_3}$ represent moles of eight-ammoniated, four-ammoniated and two-ammoniated CaCl_2 , respectively. The reversible reaction between ammoniated CaCl_2 and NH_3 can be given in Equation 20, which represents the final reactant and product amounts related to the ammonia conversion for the reaction of $\text{CaCl}_2 \cdot (2 \leftrightarrow 4)\text{NH}_3$.

<i>RXN</i>	$\text{CaCl}_2 \cdot 2\text{NH}_3$	+	2NH_3	←	$\text{CaCl}_2 \cdot 4\text{NH}_3$	
<i>Initial</i>	$n0_{\text{CaCl}_2 4\text{NH}_3}$		$n0_{\text{NH}_3}$		$n0_{\text{CaCl}_2 8\text{NH}_3}$	
<i>Change</i>	$+n0_{\text{NH}_3} \cdot \frac{X}{2}$		$-n0_{\text{NH}_3} \cdot \frac{X}{2}$		$+n0_{\text{NH}_3} \cdot \frac{X}{2}$	20
<i>Final</i>	$n0_{\text{NH}_3}(\sigma_2 - \frac{X}{2})$		$n0_{\text{NH}_3}(1 - \frac{X}{2})$		$n0_{\text{NH}_3}(\sigma_4 + \frac{X}{2})$	

In Equation 20, σ_2 is the ratio of initial moles of $\text{CaCl}_2 \cdot 2\text{NH}_3$ and initial ammonia mole and σ_4 is the ratio of initial moles of $\text{CaCl}_2 \cdot 4\text{NH}_3$ and initial ammonia mole. Similarly, the reversible reaction between $\text{CaCl}_2 \cdot 4\text{NH}_3$ and $\text{CaCl}_2 \cdot 8\text{NH}_3$ can be given in Equation 21.

RXN	$\text{CaCl}_2 \cdot 4\text{NH}_3$	+	4NH_3	\leftrightarrow	$\text{CaCl}_2 \cdot 8\text{NH}_3$	
Initial	$n0_{\text{CaCl}_2 4\text{NH}_3}$		$n0_{\text{NH}_3}$		$n0_{\text{CaCl}_2 8\text{NH}_3}$	
Change	$+n0_{\text{NH}_3} \cdot \frac{X}{4}$		$-n0_{\text{NH}_3} \cdot \frac{X}{4}$		$+n0_{\text{NH}_3} \cdot \frac{X}{4}$	21
Final	$n0_{\text{NH}_3}(\sigma_4 - \frac{X}{4})$		$n0_{\text{NH}_3}(1 - \frac{X}{4})$		$n0_{\text{NH}_3}(\sigma_8 + \frac{X}{4})$	

The conversion of ammonia can be expressed as;

$$X_{\text{NH}_3} = 1 - \frac{P}{P_0} \quad 22$$

In Equation 22, P is the bulk ammonia pressure in the reactor, and P₀ is the initial ammonia pressure supplied to the reactor. The complex reactive system is believed to be suitable for the Langmuir-Hinshelwood model. In this model, gas molecules strike the solid surface because of their kinetic energy, and a fraction of these molecules adhere to the solid surface. While some molecules bond with the solid surface, some gas molecules are separated from the solid surface due to their kinetic, rotational, and vibrational energy. The reaction rate for the entire system is determined by evaluating the adhesion of gas molecules to the surface of the solid and their separation from the solid surface (Smith, 1987). The suggested rate expressions for $\text{CaCl}_2 \cdot (4 \leftrightarrow 8)\text{NH}_3$ and $\text{CaCl}_2 \cdot (2 \leftrightarrow 4)\text{NH}_3$ reactive systems are given in Equations 23 and Equation 24, respectively. Here, the first term represents the adsorption reaction and expresses how many striking gas molecules adhere to the surface. The second term represents the desorption reaction and expresses the number of molecules leaving the surface.

$$\frac{d\theta_{\text{CaCl}_2 8\text{NH}_3}}{dt} = k_{a(4-8)}P^\alpha(1 - \theta_{\text{CaCl}_2 8\text{NH}_3})^\beta - k_{d(4-8)}\theta_{\text{CaCl}_2 8\text{NH}_3}^\gamma \quad 23$$

$$\frac{d\theta_{\text{CaCl}_2 4\text{NH}_3}}{dt} = k_{a(2-4)}P^\alpha(1 - \theta_{\text{CaCl}_2 4\text{NH}_3})^\beta - k_{d(2-4)}\theta_{\text{CaCl}_2 4\text{NH}_3}^\gamma \quad 24$$

In Equations 23 and 24, k_a and k_d represents adsorption and desorption rate constants, respectively, and α, β , and γ are reaction expression coefficients. Rate constant terms are also defined according to Arrhenius's Law given by:

$$k_a = A_a \cdot \exp(-Ea_a/RT) \quad 25$$

$$k_d = A_d \cdot \exp(-Ea_d/RT) \quad 26$$

where A_a and A_d are pre-exponential factors and Ea_a and Ea_d are activation energies for adsorption and desorption reactions, respectively. Combining Equation 18 through Equation 26, the reaction kinetic model between ammonia and CaCl_2 can be defined by Equation 27 and Equation 28;

$$\begin{aligned} \frac{d\theta_{\text{CaCl}_2 8\text{NH}_3}}{dt} = & A_{a(4-8)} \exp(-Ea_{a(4-8)}/RT) P^\alpha (1 - \theta_{\text{CaCl}_2 8\text{NH}_3})^\beta \quad 27 \\ & - A_{d(4-8)} \exp(-Ea_{d(4-8)}/RT) \theta_{\text{CaCl}_2 8\text{NH}_3}^\gamma \end{aligned}$$

$$\begin{aligned} \frac{d\theta_{\text{CaCl}_2 4\text{NH}_3}}{dt} = & A_{a(2-4)} \exp(-Ea_{a(2-4)}/RT) P^\alpha (1 - \theta_{\text{CaCl}_2 4\text{NH}_3})^\beta \quad 28 \\ & - A_{d(2-4)} \exp(-Ea_{d(2-4)}/RT) \theta_{\text{CaCl}_2 4\text{NH}_3}^\gamma \end{aligned}$$

When Equations 18 through 28 are combined, reaction rate expressions based on molar ratio, temperature, and initial pressure can be obtained as given in Equation for reactions $\text{CaCl}_2 \cdot (4 \leftrightarrow 8)\text{NH}_3$ and $\text{CaCl}_2 \cdot (2 \leftrightarrow 4)\text{NH}_3$, respectively.

$$\begin{aligned} \frac{d\theta_{\text{CaCl}_2 8\text{NH}_3}}{dt} = & A_{a(4-8)} \exp\left(\frac{-Ea_{a(4-8)}}{RT}\right) P_0^\alpha (1 - 4\sigma_4 + 4\theta_{\text{CaCl}_2 8\text{NH}_3}(\sigma_8 \\ & + \sigma_4))^\alpha (1 - \theta_{\text{CaCl}_2 8\text{NH}_3})^\beta \quad 29 \\ & - A_{d(4-8)} \exp(-Ea_{d(4-8)}/RT) \theta_{\text{CaCl}_2 8\text{NH}_3}^\gamma \end{aligned}$$

$$\begin{aligned} \frac{d\theta_{\text{CaCl}_2 4\text{NH}_3}}{dt} = & A_{a(2-4)} \exp\left(\frac{-Ea_{a(2-4)}}{RT}\right) P_0^\alpha (1 - 2\sigma_4 \\ & + 2\theta_{\text{CaCl}_2 8\text{NH}_3}(\sigma_4 + \sigma_2))^\alpha (1 - \theta_{\text{CaCl}_2 4\text{NH}_3})^\beta \quad 30 \\ & - A_{d(2-4)} \exp\left(\frac{-Ea_{d(2-4)}}{RT}\right) \theta_{\text{CaCl}_2 4\text{NH}_3}^\gamma \end{aligned}$$

3.6 Analysis Method

Adsorbed ammonia amount was calculated by the volumetric method. Pressure decrease during the adsorption reaction or pressure increase during the desorption reaction were used to calculate adsorbed/desorbed ammonia amount by using the ideal gas law. The conversion was calculated at each ammonia feeding or vacuum steps, and conversion versus time plots were obtained. From the best-fitted polynomial equations, the derivatives of the curves were obtained as the reaction rates.

First, NLR analysis was done to obtain reaction rate constants and kinetic parameters in Equations 23 and 24. Based on the initial estimated values, Polymath gives the calculated values with 95% CI and R^2 . The 95% CI should be smaller for a good fit, while the R^2 should be higher than 0.6. Moreover, Polymath gives three plots; residual plot, normal probability plot, and comparison of experimental and calculated values plot. The data points of “calculated reaction rates-experimental reactions rates” (residuals) should be randomly distributed to the reference line. In addition to the residual plots, probability plots were considered in the analysis. It shows the normal distribution when the data points lie on the reference line. During the analysis, the outlier data points were detected with the help of these curves, and the best matches were obtained.

After calculating the adsorption/desorption reaction rate constants and kinetic parameters, pre-exponential factors and activation energies were calculated according to Arrhenius's Law given in Equations 25 and 26. Finally, these values were used as initial guesses, and the temperature-dependent reaction rate kinetics given in Equations 27 and 28 were adapted to the NLR analysis in Polymath. The same procedure was followed in the analysis as described above, and kinetic parameters were obtained for these reactive systems.

3.7 Model Development

There are some models for solid-gas heterogeneous reactions. These can be classified as the shrinking core, continuous, and grain models. One of the earliest models which Ramachandran and Doraiswamy proposed in 1982 is the shrinking core model. According to this model, the reaction occurs at the particle's external surface. As the reaction proceeds, the particle shrinks but leaves behind an ash layer. It assumes that there is a sharp interface for the reaction, and this sharp interface moves through the center of the particle during the reaction. In other words, there will be an unreacted core during the reaction, which diminishes as time progress while the ash layer diameter (initial diameter of the particle) remains constant. While the gaseous product reaches the surface of this unreacted core, it comes across with some limitations because of the resistances, which are chemical reactions, diffusion in the product layer, heat transport from the reaction interface, and diffusion in the external layer. These limitations are crucial to define the system. In the continuous reaction model, gaseous reactants diffuse through the porous particle, and the reaction occurs throughout the whole particle. The limitations can be defined as chemical reactions, diffusion in the porous particle, heat transport in the particle, and diffusion in the external gas film. Grain models describe the system in which smaller solid particles form the solid particle, which is very useful for the system in which a pellet is formed by the compaction of fine-sized grains (Ramachandran & Doraiswamy, 1982), given in Figure 12 (Yake, 1980).

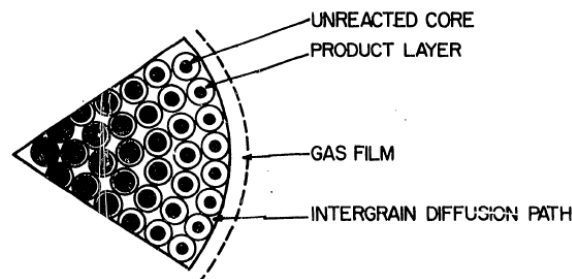


Figure 12. Description of grain model

According to this model, small particles, which are called grains, are non-porous; however, the formed particle has a void fraction due to the space between small particles. As in the continuous model, the reaction takes place in the entire pellet, while in the grain scale, the reaction occurs according to the shrinking core model. The main difference between the continuous and grain models is that the grain model assumes that small particles form the solid pellet with spaces between them. On the other hand, the continuous model assumes that the pellet is formed with a continuous solid phase with porous space. Moreover, the structural change in the solid particle is attributed to the change in each solid grain in the grain model, while it is attributed to the change in the geometrical variation of the pores in the continuous reaction model (Dai, 2017).

Rather than the shrinking core model or continuous reaction model, the particle/pellet model (grain model) is selected as the model represents the phenomena during the solid/gas reaction in this system. The reason behind this selection is that the shrinking core model needs many parameters, some of which cannot be obtained experimentally. These theory-based parameters increase the percentage of error between theoretical and experimental results. In the model, the reaction occurs at the grain level, and heat and mass transfer occur at the pellet level.

The model was developed for a slab pellet that contains spherical grains. At $t=0$, the valve between the small ammonia tank and the chamber opened, and ammonia was allowed into the chamber, and then the valve was closed. As ammonia was supplied to the chamber, it diffused through the pellet and reacted with the metal salt. During the reaction, since the molar volume of the product was almost twice the molar volume of the reactant, individual grain volume increased, leading to an increase in pellet volume. This increase also changed the parameters related to pellet structure, such as pellet density, thermal conductivity, and heat capacity. Besides, ammonia pressure decreased inside the chamber due to diffusion and reaction. But also, when the pellet volume increased, the available volume for the ammonia decreased, which led to increase in ammonia pressure inside the container. Therefore, ammonia

pressure inside the chamber was calculated at each time interval. The illustration of the system is given in Figure 13.

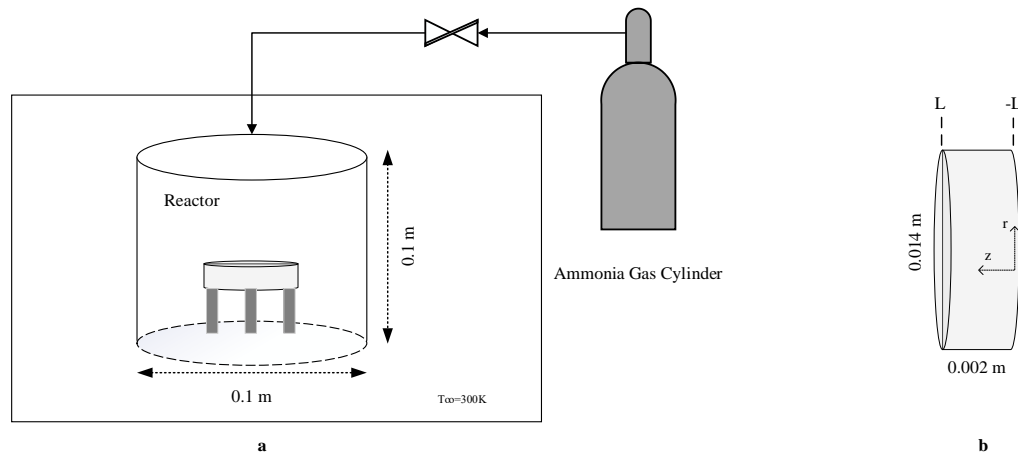


Figure 13. Schematic representation of the reactive system

The assumptions for the system are as follows:

- Radial heat and mass transfers are neglected,
- Grains are spherical and have uniform size and shape,
- The number of grains in each space interval is constant,
- The external mass transfer is negligible,
- The void fraction is constant,
- The mass transfer is mass diffusion, which is in the z-direction only,
- The thermal conductivity of ammonia and metal salts is constant,
- Ammonia is assumed to be an ideal gas, and density calculation is done accordingly,
- Pellet density, thermal conductivity, and heat capacity are calculated according to the volume averaging method,
- The expansion space of the solid particles is large enough; therefore, agglomeration is neglected.

3.8 Slab Coordinates

Slab shape pellets were obtained by compression; therefore, the model equations were derived for slab geometry.

3.8.1 Heat Transfer Equation

The model was developed for slab geometry in which time and position were the dependent variables. The model was in one-dimensional geometry for unsteady state. In Figure 14, the geometry of the pellet is given.

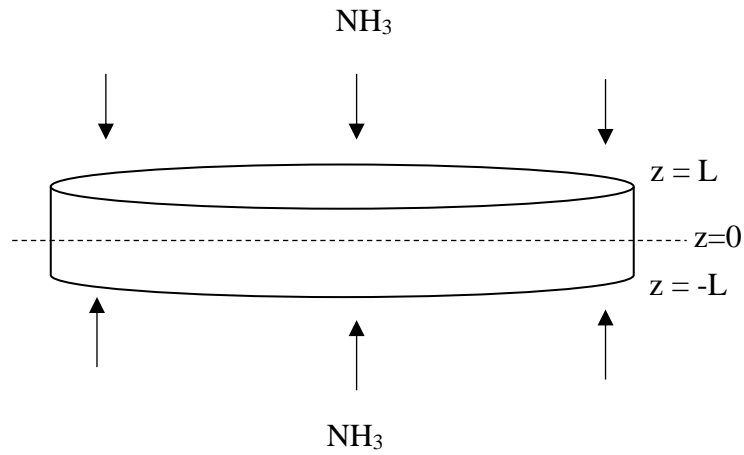


Figure 14. Slab pellet geometry

The temperature distribution was assumed to be only in the axial direction. For the selected shell, there was heat conduction in the shell at point z and conduction out at point $z+\Delta z$, and there was heat generation because of the reaction in the entire shell. This description led to Equation 31.

$$e_z(\pi r^2)|_z - e_z(\pi r^2)|_{z + \Delta z} - S_0(\pi r^2 \Delta z) \cdot \Delta H_{rxn} = \frac{d}{dt} (\rho_{sys} C_{p,sys} \pi r^2 \Delta z) \quad 31$$

Dividing by $(\pi r^2 \Delta z)$ and taking the limit as $\Delta z \rightarrow 0$, governing equation for the heat transport was obtained as given in Equation 32.

$$\begin{aligned} \frac{d}{dz} \left[k_{eff}(x(t, z)) \frac{dT(t, z)}{dz} \right] + S_0(x(t, z)) \Delta H_{rxn} & \quad 32 \\ & = \frac{d}{dt} (\rho_{sys}(x(t, z)) C_{p,sys}(x(t, z), T) T(t, z)) \end{aligned}$$

In Equation 32, k_{eff} is system effective thermal conductivity, ρ_{sys} is system density, $C_{p,sys}$ is system heat capacity and S_0 is the energy term of the reaction. Heat generation during the adsorption reaction is related to the heat of reaction and is given in Equation 33.

$$S_0 = \delta N_{salt} \frac{dx}{dt} \quad 33$$

Where δ is the stoichiometric coefficient and N_{salt} is the number of moles per unit volume of the reactive medium. System parameters were calculated based on the volume averaging method as given in Equations 34, 35, and 36. In heat capacity and density calculations, ammonia was neglected since it had a very low value.

$$\rho_{sys} = \rho_{reactant} \frac{m_{reactant}}{m_{total,solid}} + \rho_{product} \frac{m_{product}}{m_{total,solid}} \quad 34$$

$$k_{eff} = k_{reactant} \frac{V_{reactant}}{V_{total,solid}} + k_{product} \frac{V_{product}}{V_{total,solid}} + k_{NH_3} \varepsilon \quad 35$$

$$C_{p,sys} = C_{p,reactant} \frac{m_{reactant}}{m_{total,solid}} + C_{p,product} \frac{m_{product}}{m_{total,solid}} \quad 36$$

3.8.1.1 Boundary Conditions for Energy Transfer

The equations were solved as axisymmetric. Hence, the z is equal to 0 and represents the center of the slab pellet. The first boundary condition implies that there is no energy flux at $z=0$.

$$at \ z = 0 \quad \frac{\partial T(t, z)}{\partial z} = 0 \quad 37$$

The second boundary condition implies that heat is transferred to the surrounding by convective heat transfer.

$$\text{at } z = L(t) \quad -k_{\text{sys}}(x(t, z)) \frac{dT(t, z)}{dz} = h_{\text{NH}_3}(t)(T(t, L) - T_{\infty}) \quad 38$$

For the convective heat transfer coefficient calculation, firstly Nusselt number was calculated according to the Churchill-Chu correlation given in Equation 39.

$$Nu = \left[0.825 + \frac{0.387 \cdot Ra^{1/6}}{\left[1 + \left(\frac{0.492}{Pr} \right)^{9/16} \right]^{8/27}} \right]^2 \quad 39$$

In Equation 39, Ra is Rayleigh number which defines the relationship between buoyancy force and viscosity, and Pr is Prandtl number which defines the relationship between thermal diffusivity and momentum diffusivity. The relations are also given in Equations 40 and 41.

$$Ra = \frac{g\beta(T_s - T_{\infty})L_c^3\rho^2 C_p}{\mu k} \quad 40$$

$$Pr = \frac{\nu}{\alpha} \quad 41$$

In Equation 40, β is the thermal expansion coefficient, T_s is surface temperature and T_{∞} is bulk temperature, L is the characteristic length ($V_{\text{body}}/A_{\text{surface}}$), and in Equation 41, ν is kinematic viscosity of the fluid and α is thermal diffusivity. Thermal expansion coefficient is a fluid property which defines the change in density with respect to temperature at constant P, and its relation is given in Equation 42.

$$\beta = -\frac{1}{\rho} \left(\frac{\partial \rho}{\partial T} \right) \Big|_P \quad 42$$

After calculating the Nusselt number, the convective heat transfer coefficient was calculated as given in Equation 43.

$$h = \frac{Nuk}{L_c} \quad 43$$

3.8.1.2 Initial Condition for Energy Transfer

Initially, the pellet temperature was equal to the water bath temperature.

$$at\ t = 0 \quad T = 318K \text{ for } CaCl_2 \cdot (2 \leftrightarrow 4)NH_3 \quad 44$$

$$at\ t = 0 \quad T = 321K \text{ for } CaCl_2 \cdot (4 \leftrightarrow 8)NH_3$$

According to governing equation and boundary conditions, second timestep temperature values were obtained. Before going further to mass transport equations, effective diffusivity was calculated, temperature effects were considered, and the following relation was used (Everson, 2011).

$$\frac{D_{eff}}{D_0} = \left(\frac{T}{T_0}\right)^{3/2} \quad 45$$

3.8.2 Mass Transport Equations

Mass transfer occurs in the z-direction only; likewise, shell balance was written as given in Equation 46.

$$NA(\pi r^2)|_z - NA(\pi r^2)|_{z + \Delta z} - S_0(\pi r^2 \Delta z) = \frac{d}{dt}(\varepsilon C_{NH_3} \pi r^2 \Delta z) \quad 46$$

The definition of mass flux led to Equation 47.

$$\frac{\partial}{\partial z} \left(D_{eff}(x(t, z)) \frac{\partial}{\partial z} \left(\frac{P(t, z)}{RT(t, z)} \right) \right) - S_0(x(t, z)) = \frac{d}{dt} \left(\frac{\varepsilon(x(t, z)) P(t, z)}{RT(t, z)} \right) \quad 47$$

When the chain rule is applied to Equation 47, the following expression given in Equation 48 was obtained as the mass transfer equation.

$$\begin{aligned}
& \frac{1}{\varepsilon} \frac{\partial}{\partial z} \left(D_{eff}(x(t, z)) \right) \frac{\partial P(t, z)}{\partial z} - \frac{2D_{eff}(x(t, z))}{T\varepsilon} \frac{\partial P(t, z)}{\partial z} \frac{\partial T(t, z)}{\partial z} \\
& - \frac{P(t, z)}{\varepsilon T(t, z)} \frac{\partial T(t, z)}{\partial z} \frac{\partial}{\partial z} \left(D_{eff}(x(t, z)) \right) \\
& - \frac{P(t, z) D_{eff}(x(t, z))}{T(t, z) \varepsilon} \frac{\partial^2 T(t, z)}{\partial z^2} \\
& + \frac{2P(t, z) D_{eff}(x(t, z))}{\varepsilon T(t, z)^2} \left(\frac{\partial T(t, z)}{\partial z} \right)^2 \\
& + \frac{D_{eff}(x(t, z))}{\varepsilon} \frac{\partial^2 P(t, z)}{\partial z^2} \\
& - \frac{4N_{salt}(x(t, z)) RT(t, z)}{\varepsilon} \frac{dx(t, z)}{dt} - \frac{P(t, z)}{\varepsilon} \frac{\partial \varepsilon(x(t, z))}{\partial t} \\
& + \frac{P(t, z)}{T(t, z)} \frac{\partial T(t, z)}{\partial t} = \frac{\partial P(t, z)}{\partial t}
\end{aligned} \tag{48}$$

3.8.2.1 Boundary Conditions for Mass Transfer

The first boundary condition implies that there is no mass flux at $z=0$.

$$at \ z = 0 \quad \frac{\partial P(t, z)}{\partial z} = 0 \tag{49}$$

The second boundary condition implies that ammonia pressure at the outer surface is equal to bulk ammonia pressure.

$$at \ z = L(t) \quad P(t, L) = P_{bulk}(t) \tag{50}$$

3.8.2.2 Initial Condition for Mass Transfer

Because of the first two reactions $\text{CaCl}_2 \cdot (0 \leftrightarrow 1)\text{NH}_3$ and $\text{CaCl}_2 \cdot (1 \leftrightarrow 2)\text{NH}_3$, ammonia gas was present in the system. For the initial pressure of ammonia, the amount of ammonia from the previous reactions was considered and taken as the

initial ammonia pressure at the beginning of the $\text{CaCl}_2 \cdot (2 \leftrightarrow 4)\text{NH}_3$ and $\text{CaCl}_2 \cdot (4 \leftrightarrow 8)\text{NH}_3$ reactions.

$$\text{at } t = 0 \quad P(t, z) = 1.93 \text{ bars for } \text{CaCl}_2 \cdot (2 \leftrightarrow 4)\text{NH}_3$$

51

$$\text{at } t = 0 \quad P(t, z) = 2.82 \text{ bars for } \text{CaCl}_2 \cdot (4 \leftrightarrow 8)\text{NH}_3$$

3.9 Analysis Method

The differential equations were solved numerically using the “Finite Difference Method”. The explicit method with central in space and forward in time was used. The discretization was given in Equations 52, 53, and 54. In these equations, Ω is used for an arbitrary parameter.

$$\frac{\partial \Omega}{\partial t} = \frac{\Omega_{i,j+1} - \Omega_{i,j}}{\Delta t} \quad 52$$

$$\frac{\partial \Omega}{\partial z} = \frac{\Omega_{i+1,j} - \Omega_{i-1,j}}{2\Delta z} \quad 53$$

$$\frac{\partial^2 \Omega}{\partial r^2} = \frac{\Omega_{i+1,j} - 2\Omega_{i,j} + \Omega_{i-1,j}}{\Delta r^2} \quad 54$$

The given equations are for equal increments. In the developed model, the increase in the pellet length was considered when the model was run for dt time. Therefore, each length increment increased proportionally to the conversion. The revised version of Equations 53 and 54 are given in Appendix -C.

3.10 Algorithm of MATLAB

1. Define constant values related to pellet and solid particle geometries, reaction kinetics parameters, constants of physico-chemical properties of metal salts and ammonia, and physico-chemical properties of metal salts and ammonia

2. Set the initial values of pellet and solid particle geometries, reaction kinetics parameters, system pressure, system temperature, equilibrium pressure, physical properties of the system (porosity and effective diffusivity), amounts of reactants and products (in mass and in mole), the volume of pellet, ammonia volume, particle number
3. Define the number of intervals and related spatial and time increments
4. Create zero matrices for all parameters according to the defined number of intervals that are defined in the 3rd item.
5. Specify initial constants and initial calculated values as the first term of the matrices defined in the 4th item.
 - 5.1. Calculate the initial value of Pr, Ra, and Nu numbers and convective heat transfer coefficient (h)
 - 5.2. Discretize the length of the pellet, total and solid volumes of pellet, reactant and product salt amount (in mole and in mass), particle number, pellet density (ρ), pellet heat capacity (C_p), and pellet thermal conductivity (k)
6. Beginning of time loop;
 - 6.1. Calculation of conversion at each spatial interval
 - 6.2. Calculation of conversion-related parameters
 - 6.3. Calculation of temperature at each spatial position
 - 6.4. Calculation of temperature-related parameters
 - 6.5. Calculation of ammonia pressure at each spatial position
 - 6.6. Calculation of ammonia pressure-related parameters
 - 6.7. Calculation of convective heat transfer coefficient
 - 6.8. Replace old values with new values
 - 6.9. Write table
7. End of time loop

CHAPTER 4

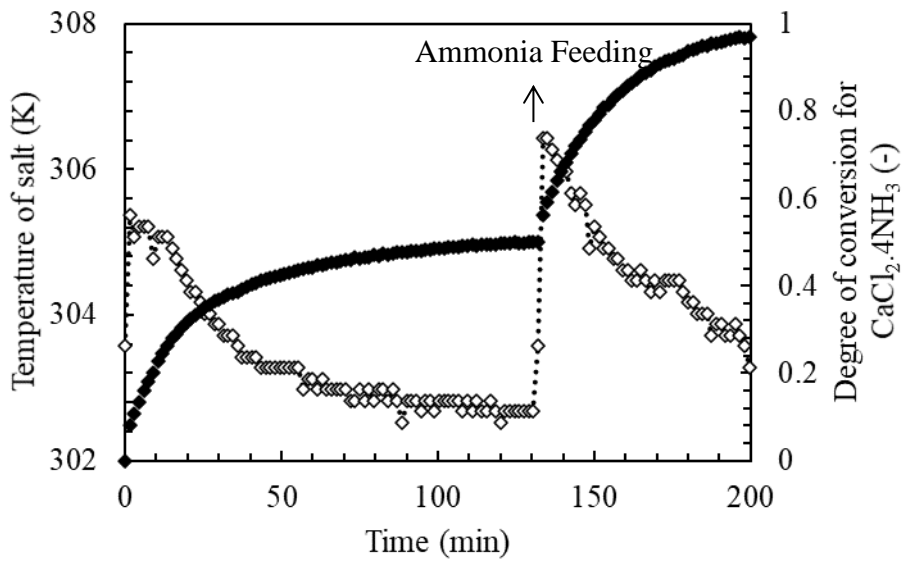
RESULTS AND DISCUSSION

4.1 Reaction Rate Kinetics Results and Discussion

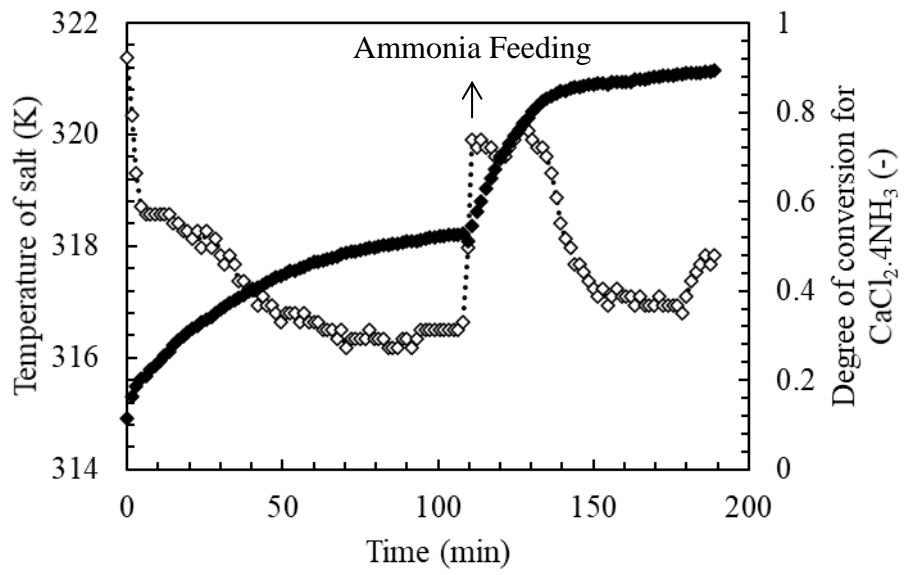
In this section, the results of the experiments for the determination of reversible reaction rate kinetics will be summarized and discussed.

4.1.1 $\text{CaCl}_2 \cdot (2 \leftrightarrow 4)\text{NH}_3$ Reaction Kinetics Results

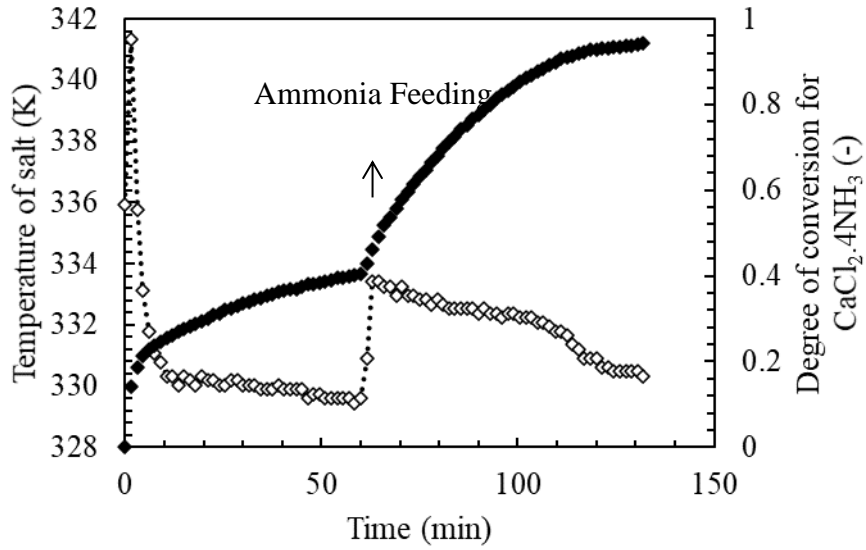
0.3 grams of anhydrous CaCl_2 was used as the first reactant in $\text{CaCl}_2 \cdot (2 \leftrightarrow 4)\text{NH}_3$ experiments. In order to avoid the simultaneous occurrence of the $\text{CaCl}_2 \cdot (2 \leftrightarrow 4)\text{NH}_3$ and $\text{CaCl}_2 \cdot (2 \leftrightarrow 4)\text{NH}_3$ reactions, the operating pressure was selected based on the equilibrium pressures at the working temperatures. The change in local temperature salt and conversion for $\text{CaCl}_2 \cdot 4\text{NH}_3$ are given in Figure 15. Each ammonia feeding is represented as arrows, described in Chapter 3.



-a-



-b-



-c-

Figure 15. Salt temperature change inside the salt (open diamonds with round dot line) and degree of conversion for $\text{CaCl}_2 \cdot 4\text{NH}_3$ (closed diamonds) with respect to time for adsorption reaction a) 30°C b) 45°C c) 55°C

In Figure 15, the closed diamonds represent the conversion of $\text{CaCl}_2 \cdot 4\text{NH}_3$ with respect to time. The conversion of $\text{CaCl}_2 \cdot 4\text{NH}_3$ reached 1 in two ammonia feedings at each temperature. Moreover, the open diamonds represent the local temperature change during the adsorption reaction. Since it was an exothermic reaction, the local temperature of the salt suddenly increased as soon as the ammonia gas was sent through the reactor. While the adsorption reaction continued, the temperature of the salt decreased smoothly because of the external cooling from the water bath, where the temperature was constant at 30°C , 45°C , and 55°C . Hence, the final temperature of the salt reached the water bath temperature at the end of each temperature.

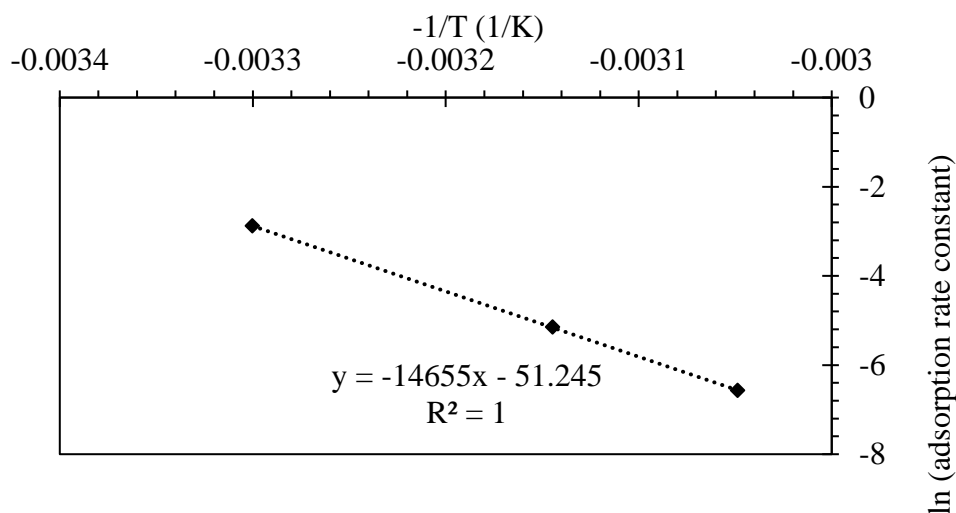
First, the Non-Linear Regression analysis was used to calculate the adsorption and desorption rate constants and the parameters α , β , and γ in Polymath software. According to the first analysis, α , β , and γ are selected as 3, 0.1, and 0.3, respectively.

The analyzed adsorption and desorption rate constants are given in Table 5. The Polymath analysis results are given in Appendix-A.

Table 5. Adsorption and desorption rate constants for 30°C, 45°C, and 55°C when α , β , and γ are 3, 0.1, and 0.3, respectively, for $\text{CaCl}_2 \cdot (2 \leftrightarrow 4)\text{NH}_3$ reaction with initial 0.3 grams of metal salt

Operating Temperature (K)	Variable	Value	95% Confidence	R ²
30°C	$k_{a(2-4)} (\text{min}^{-1}\text{bar}^{-3})$	0.0570	4.8×10^{-3}	0.95
	$k_{d(2-4)} (\text{min}^{-1})$	0.0120	1.9×10^{-3}	
45°C	$k_{a(2-4)} (\text{min}^{-1}\text{bar}^{-3})$	0.0060	2.1×10^{-3}	0.68
	$k_{d(2-4)} (\text{min}^{-1})$	0.0150	7.5×10^{-3}	
55°C	$k_{a(2-4)} (\text{min}^{-1}\text{bar}^{-3})$	0.0014	1.9×10^{-4}	0.93
	$k_{d(2-4)} (\text{min}^{-1})$	0.0200	3.6×10^{-3}	

In Figure 16, Arrhenius plots are given for adsorption and desorption reaction rate constants. The slope of $\ln(\text{reaction rate constant})$ versus $-1/T$ gives the E/R , and the intercept gives the $\ln(A)$.

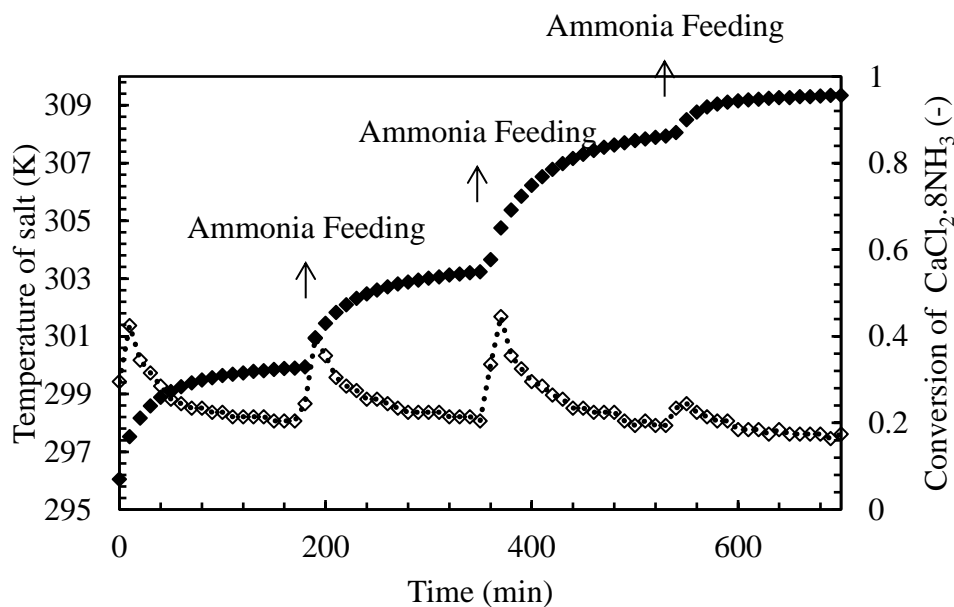


-a-

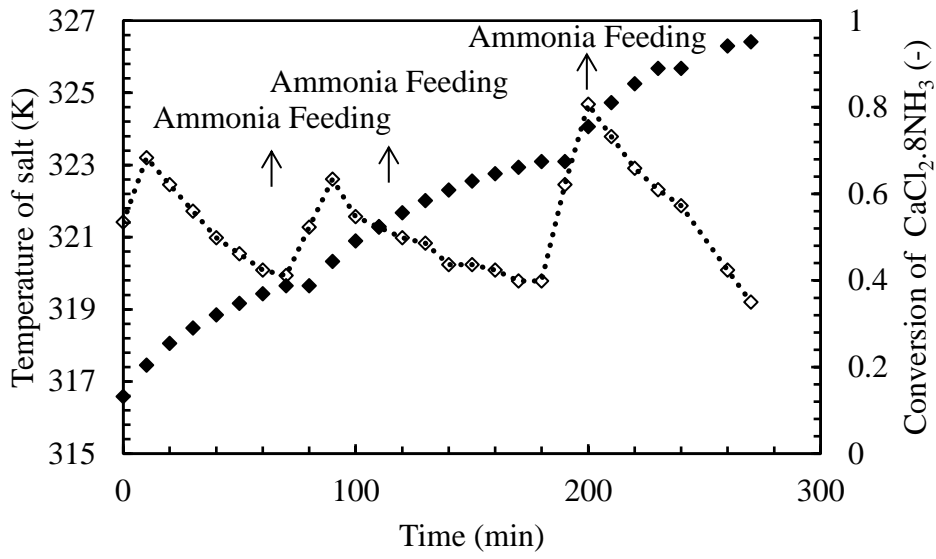
Except for the second ammonia feeding at 25°C, the experimental and calculated reaction rates show good agreement.

4.1.2 $\text{CaCl}_2 \cdot (4 \leftrightarrow 8)\text{NH}_3$ Reaction Kinetics Results

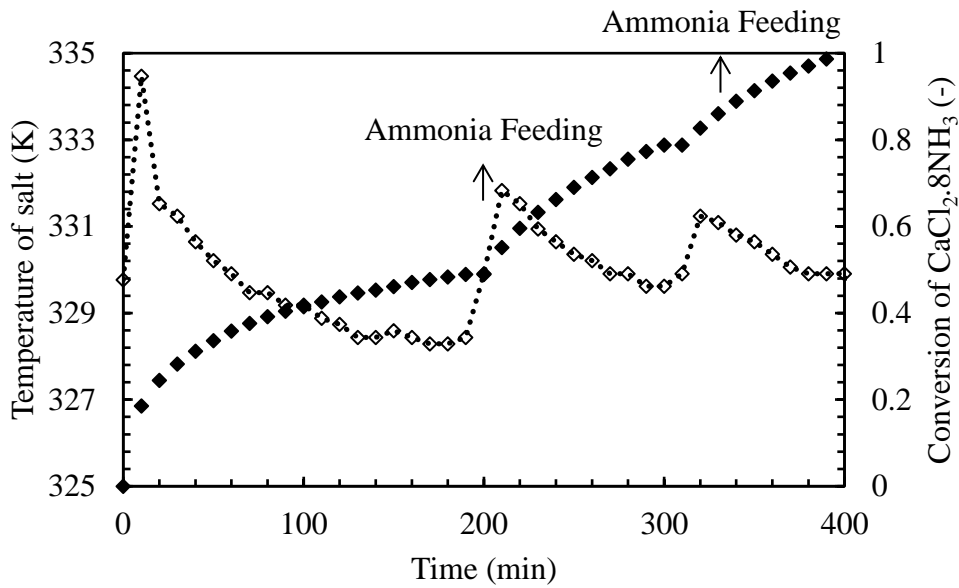
$\text{CaCl}_2 \cdot (4 \leftrightarrow 8)\text{NH}_3$ adsorption reaction was followed by the $\text{CaCl}_2 \cdot (2 \leftrightarrow 4)\text{NH}_3$ adsorption reaction. The experiments were conducted with 0.5 grams of initial CaCl_2 as the first reactant. Ammonia flush and adsorption/desorption experiments were carried out as described in Chapter 3. Changes in local temperature salt and conversion for $\text{CaCl}_2 \cdot 8\text{NH}_3$ are given in Figure 20.



-a-



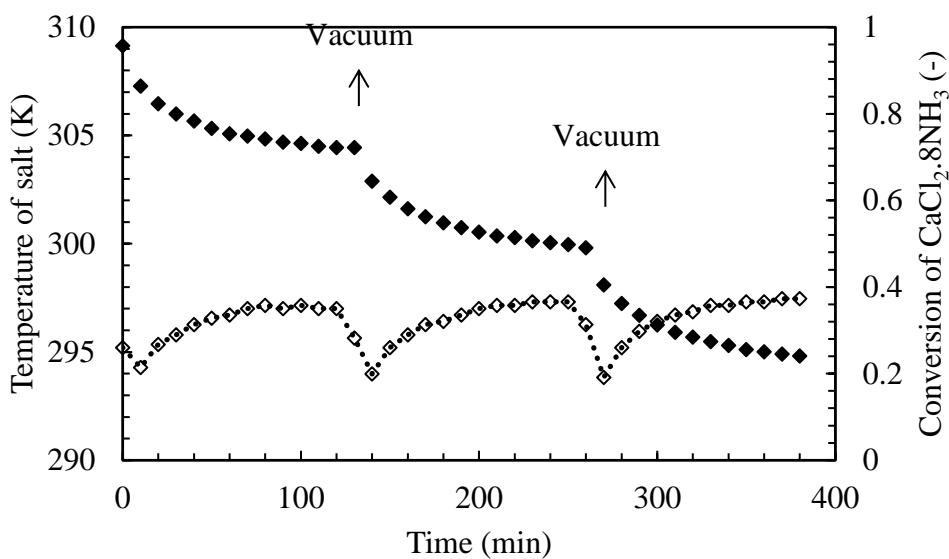
-b-



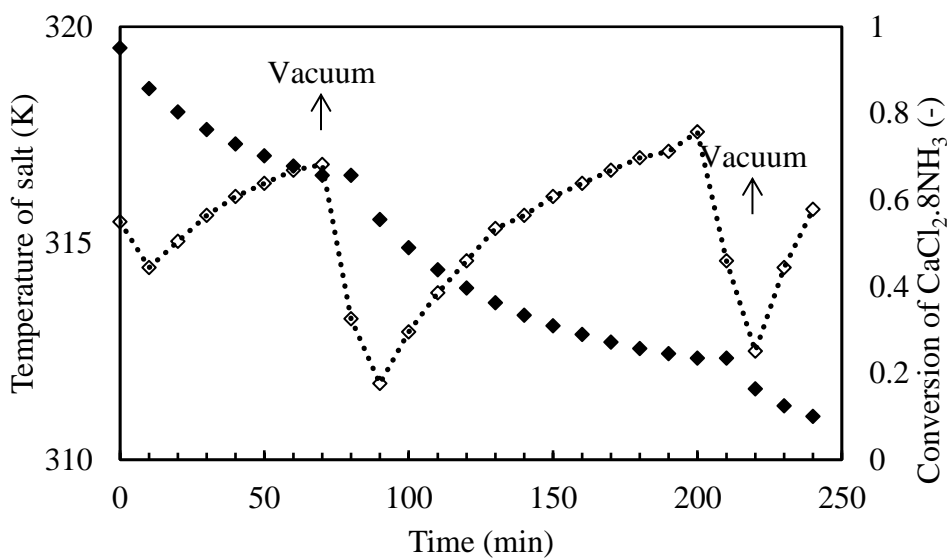
-c-

Figure 20. Salt temperature (open diamonds with round dot line) and degree of conversion for $\text{CaCl}_2 \cdot 8\text{NH}_3$ (closed diamonds) for adsorption reaction at 30°C , 45°C and 55°C , respectively

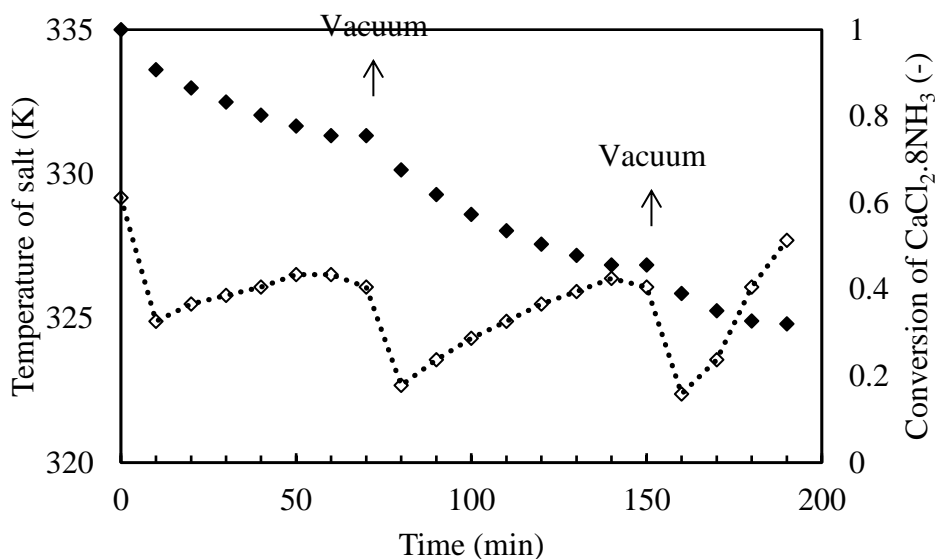
As observed in Figure 20, the local salt temperature increased suddenly as soon as the ammonia was sent to the reactor. Because of the constant water bath temperature, the salt temperature decreased down to the water bath temperature.



-a-



-b-



-c-

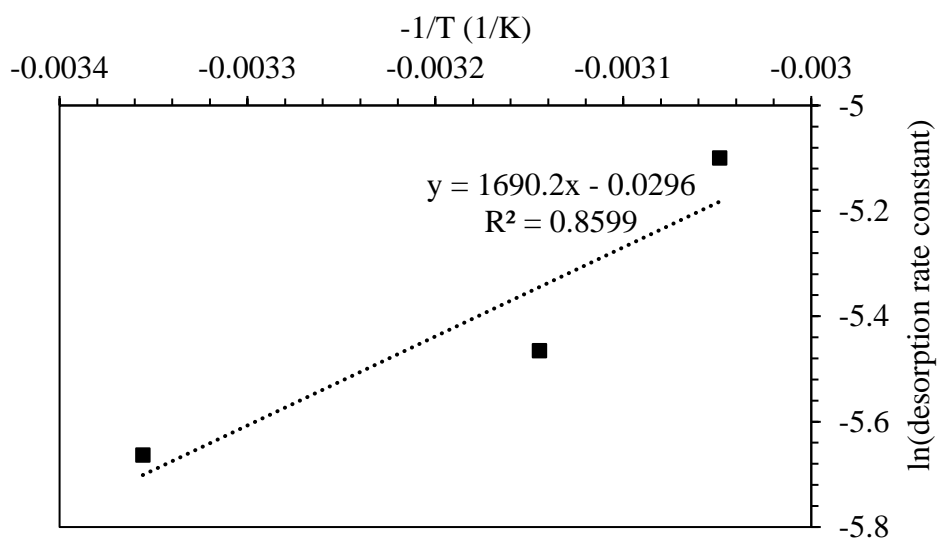
Figure 21. Salt temperature (open diamonds with round dot line) and degree of conversion for CaCl₂.8NH₃ (closed diamonds) for desorption reaction at 30°C, 45°C, and 55°C, respectively

In Figure 21, local salt temperature change and conversion of CaCl₂.8NH₃ are given for the desorption reaction. Since the desorption reaction is endothermic, salt temperature first decreases as soon as the ammonia pressure decreases. As observed in the adsorption reaction, salt temperature eventually equals to the water bath temperature in the desorption reaction. For the kinetic analysis, the same procedure was followed for the CaCl₂ · (4 ↔ 8)NH₃ reaction. According to the first analysis, α, β, and γ are selected as 3, 0.5, and 0.2, respectively. The adsorption reaction rates were first used to calculate adsorption and desorption reaction rate constants. The calculated values according to NLR analysis in Polymath are given in Table 7.

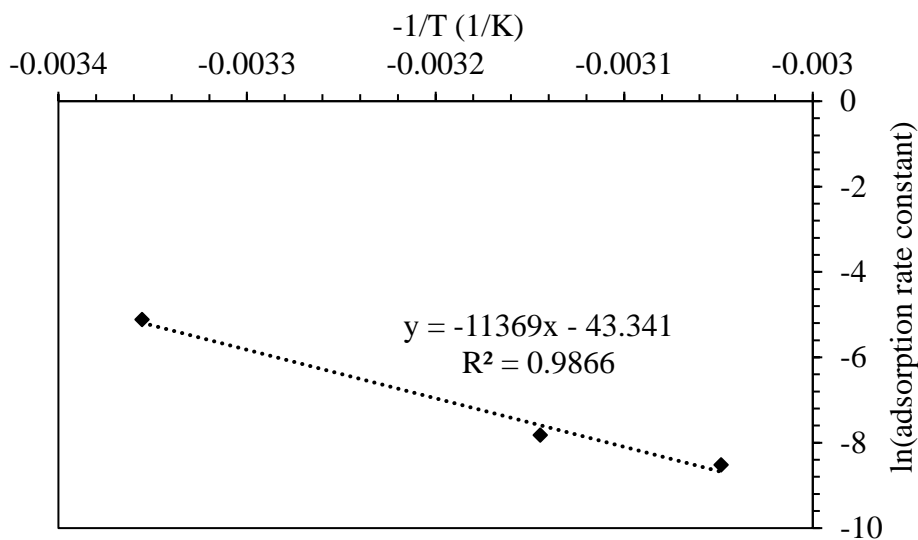
Table 7. Adsorption and desorption rate constants for 30°C, 45°C and 55°C when α , β and γ are 3, 0.5 and 0.2, respectively for $\text{CaCl}_2 \cdot (4 \leftrightarrow 8)\text{NH}_3$ reaction with initial 0.5 grams of metal salt

Operating Temperature (K)	Variable	Value	95% Confidence	R ²
25°C	$k_{a(4-8)}(\text{min}^{-1}\text{bar}^{-3})$	0.0060	4.1×10^{-4}	0.92
	$k_{d(4-8)}(\text{min}^{-1})$	0.0035	3.5×10^{-4}	
45°C	$k_{a(4-8)}(\text{min}^{-1}\text{bar}^{-3})$	0.0004	3.1×10^{-5}	0.95
	$k_{d(4-8)}(\text{min}^{-1})$	0.0042	6.5×10^{-4}	
55°C	$k_{a(4-8)}(\text{min}^{-1}\text{bar}^{-3})$	0.0002	2.4×10^{-5}	0.78
	$k_{d(4-8)}(\text{min}^{-1})$	0.0061	1.1×10^{-3}	

According to the calculated reaction rate constants for adsorption and desorption reactions, Arrhenius plots are given in Figure 22.



-a-



-b-

Figure 22. Arrhenius plots for $\text{CaCl}_2 \cdot (4 \leftrightarrow 8)\text{NH}_3$ reaction a) Desorption Arrhenius plot b) Adsorption Arrhenius plot

From the Arrhenius plots, pre-exponential factors and activation energies of adsorption and desorption reactions were calculated, and these values were used as the initial values for the NLR analysis done in Polymath.

Table 8. Apparent activation energies and pre-exponential factors of adsorption and desorption rate constants based on the Arrhenius plots and NLR analysis on Polymath and Minitab for $\text{CaCl}_2 \cdot (4 \leftrightarrow 8)\text{NH}_3$ reaction

Analysis Tool	$A_{a(4-8)}$ ($\text{min}^{-1}\text{bar}^{-3}$)	$E_a, \text{app}_{a(4-8)}$ (J/mol)	$A_{d(4-8)}$ (min^{-1})	$E_a, \text{app}_{d(4-8)}$ (J/mol)
Arrhenius Plots	1.50×10^{-19}	-94521	0.98	14050
Polymath Analysis	2.64×10^{-18}	-88130	3.44	16500

CHAPTER 5

CONCLUSION

In the scope of this study, $\text{CaCl}_2 \cdot (2 \leftrightarrow 4)\text{NH}_3$ and $\text{CaCl}_2 \cdot (4 \leftrightarrow 8)\text{NH}_3$ reactive systems were investigated in terms of reaction kinetics. Different from the literature where the reaction rates were expressed for adsorption and desorption individually, reversible reaction rates were suggested. This study's suggested reaction rate expression was based on the Langmuir-Hinshelwood model. In this model, the net reaction rate is expressed as the summation of the adsorption and desorption reactions. The net reaction rate depends on the vacant site's availability, the initial ammonia pressure, and the energy of the gas molecules. The net effect of equilibrium pressure is not integrated into the reversible reaction rate. The dependency of the reaction rate to the equilibrium conditions is obtained from the desorption term in the case of the adsorption reaction, and it is obtained from the adsorption term in the case of the desorption reaction. Therefore, at the equilibrium, different from the literature, the adsorption reaction rate is not zero; however, the adsorption and desorption reaction rates are equal to each other.

In order to evaluate the reaction rate kinetic parameters, pre-exponential factors, and activation energies, reaction kinetics experiments were conducted. For this purpose, an experimental setup was demonstrated, which contains a reactor, gas cylinder, and vacuum pump. The kinetic experiments were done with the powder CaCl_2 to eliminate the heat and mass transfer limitations during the reaction. The first reaction was conducted with 0.5 grams of initial CaCl_2 powder. It is known that after the first reaction, the structure of the metal salt changes, and the volume increases because of the difference in the molar volumes of the reactants and products. After the first cycle, the reaction rate becomes independent of the initial solid particle, the number of cycles, and the conversion. Therefore, before the kinetic experiments, metal salt was first flushed with ammonia. The reaction was conducted at three temperatures,

30°C, 45°C, and 55°C, to evaluate the rate constant parameters. The NLR analysis was done firstly to evaluate adsorption and desorption rate constants which were then used for the Arrhenius plots for pre-exponential factors and activation energies. Then the calculated values were integrated into the NLR analysis as the first guess values, and these were also calculated with the whole data set, including the desorption reaction rates for the reaction of $\text{CaCl}_2 \cdot (4 \leftrightarrow 8)\text{NH}_3$. The experiments were also repeated with 0.3 grams of initial metal salt, and the experimental and calculated results were compared. According to the NLR analysis, pre-exponential factors were obtained as $7.06 \cdot 10^{-22}$ and 102 for adsorption and desorption terms, respectively, for the $\text{CaCl}_2 \cdot (2 \leftrightarrow 4)\text{NH}_3$ reaction. These values are obtained as $2.64 \cdot 10^{-18}$ and 3.44, respectively, for the $\text{CaCl}_2 \cdot (4 \leftrightarrow 8)\text{NH}_3$ reaction. Also, adsorption and desorption activation energies were obtained as $-115600 \text{ J mol}^{-1}$ and 23310 J mol^{-1} , respectively, for the $\text{CaCl}_2 \cdot (2 \leftrightarrow 4)\text{NH}_3$ reaction. Moreover, these were obtained as $-88130 \text{ J mol}^{-1}$ and 16500 J mol^{-1} for adsorption and desorption terms for $\text{CaCl}_2 \cdot (4 \leftrightarrow 8)\text{NH}_3$ reaction. The experimental and calculated reaction rates were observed to be compatible with each other except for the desorption reaction at 25°C. This deviation was believed to be the presence of the physisorption.

The metal salts are used in the pellet forms in the CHP and hydrogen storage applications in order to increase the NH_3 sorption capacity. Therefore, in the second part of this study, $\text{CaCl}_2\text{-NH}_3$ reactive system was investigated when the CaCl_2 was used in the pellet form. The reactive system was considered taking heat and mass transport phenomena into account coupled with reversible chemical reactions. The governing equations were developed by using the obtained reversible reaction expression in the first part of this study. Since the differential equations are not solved analytically, a numerical solution was required, and hence, Finite Difference Method was used. The equations were solved using MATLAB software. Also, different from the literature, the increase in the pellet volume was considered in the model, and the boundary conditions are written accordingly. In order to compare the simulation results, the pellet experiments were done at 318 K and 321 K. It was noted that the volume of the pellet increased by its length while the diameter changed

slightly. Therefore, the model was developed by considering the change in the length. The simulation results were first obtained for the $\text{CaCl}_2 \cdot (2 \leftrightarrow 4)\text{NH}_3$ reaction, where the initial ammonia pressure in the pellet and initial bulk ammonia pressure was 1.93 bars. The effective diffusivity was calculated based on the literature value, and a more adopted value was obtained as $2 \cdot 10^{-5} \text{ m}^2 \text{ s}^{-1}$. The porosity of the system was assumed as 0.1. In the simulation, the porosity and effective diffusivity change was eliminated. Experimentally obtained bulk ammonia pressure changes with respect to time were compared with the simulation results. It was observed that the experimental and simulation results were compatible with each other in 700 seconds. However, after 700 seconds, deviation in the results was observed, which was attributed to the constant effective diffusivity in the simulation. It was deduced that the effective diffusivity decreases as the adsorption reaction progresses because the space between the voids decreases due to the increase in the volume of the small grains. Also, a slight temperature distribution was observed, which is an expected result since the system was mentioned as heat transfer limited in the literature. Compared to the literature, the temperature distribution was smaller, which may be due to the small pellet length in this study. Secondly, the reactive system of $\text{CaCl}_2 \cdot (4 \leftrightarrow 8)\text{NH}_3$ was studied. In this case, the initial ammonia pressure in the pellet was much smaller than the initial bulk ammonia pressure. The experimental bulk ammonia pressure change and simulation results are compatible. The deviation observed in the former reaction was not seen in this case because the slab pellet was dispersed during the reaction. Therefore, effective diffusivity may not decrease experimentally in this case and become more similar to the simulation. The dispersion of the pellet showed that for the CHP and hydrogen storage applications, pellets obtained by compression pressure lower than 60 kN are crucial because of the repeatability and reproducibility of the system. When the compression pressure is lowered, the amount of CaCl_2 would be decreased if the net volume is the same, and this decrease will lead to lower sorption capacity; however, for the system to have a higher number of cycles, it is significant. On the other hand, lower compression force will lead to a higher permeability that enhances the mass transfer

inside the pellet. Also, the temperature distribution was observed; however, it was not clear as the former reaction because the reaction rate was slower than that of $\text{CaCl}_2 \cdot (2 \leftrightarrow 4)\text{NH}_3$ reaction. Hence, as the reaction progressed, while the temperature of the pellet increased because of the exothermicity of the reaction, it also cooled down to the water bath temperature. Therefore, the temperature of the salt did not increase as much as in the former case. On the other hand, a slight pressure gradient was observed in this case because of the difference in the initial ammonia pressure in the pellet and initial bulk ammonia pressure.

In conclusion, the reactive systems of $\text{CaCl}_2 \cdot (2 \leftrightarrow 4)\text{NH}_3$ and $\text{CaCl}_2 \cdot (4 \leftrightarrow 8)\text{NH}_3$ were well represented by reversible reaction rate expressions, suitable for the Langmuir-Hinshelwood model. Moreover, the reactive system was well established by a theoretical model considering heat and mass transport phenomena with the obtained reversible reaction rate kinetic with adapting the structural change by MATLAB software.

REFERENCES

- Abedin, A. H. (2011). A Critical Review of Thermochemical Energy Storage Systems. *The Open Renewable Energy Journal*, 4(1), 42–46. <https://doi.org/10.2174/1876387101004010042>
- Aoki, T., Miyaoka, H., Inokawa, H., Ichikawa, T., & Kojima, Y. (2015). Activation on Ammonia absorbing reaction for magnesium chloride. *The Journal of Physical Chemistry*, 119, 26296-26302. doi:10.1021/acs.jpcc.5b07965
- Aydin, D., Casey, S. P., & Riffat, S. (2015). The latest advancements on thermochemical heat storage systems. *Renewable and Sustainable Energy Reviews*, 41, 356–367. <https://doi.org/10.1016/j.rser.2014.08.054>
- Azoumah, Y., Neveu, P., & Mazet, N. (2007). Optimal design of thermochemical reactors based on constructal approach. *AIChE Journal*, 53(5), 1257-1266. doi:10.1002/aic.11152
- Carling, R. W. (1981). Dissociation pressures and enthalpies of reaction in $MgCl_2 \cdot nH_2O$ and $CaCl_2 \cdot nH_2O$. *Journal of Chemical Thermodynamics*, 13, 503-512.
- Chan, C. W., Ling-Chin, J., & Roskilly, A. P. (2013). A review of chemical heat pumps, thermodynamic cycles and thermal energy storage technologies for low grade heat utilisation. *Applied Thermal Engineering*, 50, 1257-1273. doi:10.1016/j.applthermaleng
- Christensen, C. H., Sørensen, R. Z., Tue Johannessen, T., Quaade, U. J., Honkala, K., Elmøe, T. D., Nørskov, J. K. (2005). Metal ammine complexes for hydrogen storage. *Journal of Material Chemistry*, 4106-4108. doi:10.1039/b511589b.
- Council, W. E. (n.d.). *World Energy Resources 2013 Survey*

- Cot-Gores, J., Castell, A., & Cabeza, L. F. (2012). Thermochemical energy storage and conversion: A-state-of-the-art review of the experimental research under practical conditions. *Renewable and Sustainable Energy Reviews*, 16(7), 5207–5224. <https://doi.org/10.1016/j.rser.2012.02.007>
- Critoph, R. E. (2012). Solid sorption cycles: A short history. *International Journal of Refrigeration*, 35(3), 490–493. <https://doi.org/10.1016/j.ijrefrig.2012.02.007>
- Dai, P. (2017). Modeling non-catalytic gas-solid reactions (Unpublished master's thesis). University of Cambridge.
- Demir, H., Mobedi, M., & Ülkü, S. (2008). A review on adsorption heat pump: Problems and solutions. *Renewable and Sustainable Energy Reviews*, 12(9), 2381–2403. <https://doi.org/10.1016/j.rser.2007.06.005>
- Dunsford, F.T., 1915. Improvements in absorption refrigerating apparatus, GB patent 17, 672. Fig. 5 e Wave Air solid sorption gas heat pump (Wave Air Corporation, 1993).
- Dutour, S., Mazet, N., Joly, J., & Platel, V. (2005). Modeling of heat and mass transfer coupling with gas–solid reaction in a sorption heat pump cooled by a two-phase closed thermosyphon. *Chemical Engineering Science*, 60(15), 4093–4104. doi:10.1016/j.ces.2005.02.046
- Elmøe, T. D., Sørensen, R. Z., Quaade, U., Christensen, C. H., Nørskov, J. K., & Johannessen, T. (2006). A high-density ammonia storage/delivery system based on Mg(NH₃)₆Cl₂ for SCR–DeNO_x in vehicles. *Chemical Engineering Science*, 61, 2618–2625. doi:10.1016/j.ces.2006.05.010
- Enibe, S. O., & Iloeje, O. C. (2000). Heat and mass transfer in porous spherical pellets of CaCl₂ for solar refrigeration. *Renewable Energy*, 20(3), 305–324. [https://doi.org/10.1016/S0960-1481\(99\)00105-6](https://doi.org/10.1016/S0960-1481(99)00105-6)
- Everson, R. C., Neomagus, H. W. J. P., & Kaitano, R. (2011). The random pore model with intraparticle diffusion for the description of combustion of char

particles derived from mineral- and inertinite rich coal. *Fuel*, 90(7), 2347–2352. <https://doi.org/10.1016/j.fuel.2011.03.012>

Faraday. (1823). XVII. On the condensation of several gases into liquids. 10.

Goetz, V., & Marty, A. (1992). A model for reversible solid-gas reactions submitted to temperature and pressure constraints: Simulation of the rate of reaction in solid-gas reactor used as chemical heat pump. *Chemical Engineering Science*, 17, 4445-4454

Han, J. H., Lee, K.-H., Kim, D. H., & Kim, H. (2000). Transformation Analysis of Thermochemical Reactor Based on Thermophysical Properties of Graphite–MnCl₂ Complex. *Industrial & Engineering Chemistry Research*, 39(11), 4127–4139. <https://doi.org/10.1021/ie991344a011>

Hastaoglu, M. A., & Abba, I. A. (1996). Modelling of multi gas/solid reactions - Effect of structural parameters. *Chemical Engineering and Technology*, 19(4), 337–346. <https://doi.org/10.1002/ceat.270190407>

Hedayat Mofidi, S. A., & Udell, K. S. (2019). Absorption Process in MgCl₂–NH₃ Thermochemical Batteries With Constant Mass Flow Rate. *Journal of Energy Resources Technology*, 141(6), 062004. <https://doi.org/10.1115/1.4042406>

Hill, C. G., Jr. (1977). *An introduction to chemical engineering kinetics and reactor design*. USA: John Wiley & Son

Huang, H. J., Wu, G. Bin, Yang, J., Dai, Y. C., Yuan, W. K., & Lu, H. B. (2004). Modeling of gas-solid chemisorption in chemical heat pumps. *Separation and Purification Technology*, 34(1–3), 191–200. [https://doi.org/10.1016/S1383-5866\(03\)00192-8](https://doi.org/10.1016/S1383-5866(03)00192-8)

Hulse, G. E. (1929). Freight Car Refrigeration by an Adsorption System Employing Silica Gel. *Refrigeration Engineering*. 17(2), 41-54

- Hummelshøj, J. S., Sørensen, R. Z., Kustova, M. Y., Johannessen, T., Nørskov, J. K., & Christensen, C. H. (2005). Generation of Nanopores during Desorption of NH₃ from Mg(NH₃)₆Cl₂. *Journal of American Chemical Society*, 128, 16-17. doi:10.1021/ja0556070
- Iwata, R., Yamauchi, T., Hirota, Y., Aoki, M., & Shimazu, T. (2014). Reaction kinetics of ammonia absorption/desorption of metal salts. *Applied Thermal Engineering*, 72(2), 244-249. doi:10.1016/j.applthermaleng.2014.07.034
- Jacobsen, H. S., Hansen, H. A., Andreassen, J. W., Shi, Q., Andreassen, A., Feidanhans'l, R., Vegge, T. (2007). Nanoscale structural characterization of Mg(NH₃)₆Cl₂ during NH₃ desorption: An in situ small angle X-ray scattering study. *Chemical Physics*
- Laidler, K. J., Meiser, J. H., & Sanctuary, B. C. (2003). *Physical Chemistry*. USA: Nelson Education.
- Lebrun, M., & Spinner, B. (1990). Models of heat and mass transfers in solid-gas reactors used as chemical heat pumps. *Chemical Engineering Science*, 45(7), 1743-1753.
- Le Pierrès, N., Mazet, N., & Stitou, D. (2007). Modelling and performances of a deep-freezing process using low-grade solar heat. *Energy*, 32(2), 154-164. doi:10.1016/j.energy.2006.02.009
- Le Pierrès, N., Driss, S., & Nathalie, M. (2008). Design of a thermochemical process for deep freezing using solar low-grade heat. *Chemical Engineering and Processing: Process Intensification*, 47(3), 484-489. doi:10.1016/j.cep.2007.01.011
- Li, T. X., Wang, R. Z., Wang, L. W., Lu, Z. S., & Wu, J. Y. (2008). Influence of mass recovery on the performance of a heat pipe type ammonia sorption refrigeration system using CaCl₂/activated carbon as compound adsorbent. *Applied Thermal Engineering*

- Li, T., Wang, R., & Wang, L. (2009). High-efficient thermochemical sorption refrigeration driven by low-grade thermal energy. *Science Bulletin*, 54(6), 885–905. doi: 10.1007/s11434-009-0117-3
- Li, T. X., Xu, J. X., Yan, T., Wang, R. Z. (2016). Development of sorption thermal battery for low-grade waste heat recovery and combined cold and heat energy storage. *Energy*, 107, 347-359. doi: 10.1016/j.energy.2016.03.126.
- Lu, H. B., Mazet, N., & Spinner, B. (1995). Modelling of gas-solid reaction - coupling of heat and mass transfer with chemical reaction. *Chemical Engineering Science*, 51, 3829-3845.
- Lyakh, M. Y., Rabinovich, O. S., Vasiliev, L. L., & Tsitovich, A. P. (2013). Improving the performance of an adsorption heat converter in condensation and evaporation of the adsorbate in sorbent pores. *Journal of Engineering Physics and Thermophysics*, 86(6), 1259-1272. doi:10.1007/s10891-013-0949-1
- Mazet, N., Amouroux, M., & Spinner, B. (1991). Analysis and experimental study of the transformation of a non-isothermal solid/gas reacting medium. *Chemical Engineering Communications*, 99, 155-174.
- Miller, E. B. (1929). Refrigeration, US Patent 1,729,081.
- Mofidi, S. A. H., & Udell, K. S. (2017). Study of Heat and Mass Transfer in MgCl₂/NH₃ Thermochemical Batteries. *Journal of Energy Resources Technology*, 139(3), 032005. <https://doi.org/10.1115/1.4035750>
- Mofidi, S. A. H., & Udell, K. S. (2019). Absorption process in MgCl₂/NH₃ thermochemical batteries with constant mass flow rate. *Journal of Energy Resources Technology*, 141(6). <https://doi.org/10.1115/1.4042406>
- Neveu, P., & Castaing, J. (1993). Solid-gas chemical heat pumps: Field of application and performance of the internal heat of reaction recovery process. *Heat Recovery Systems and CHP*, 13(3), 233–251. [https://doi.org/10.1016/0890-4332\(93\)90014-M](https://doi.org/10.1016/0890-4332(93)90014-M)

- Neveu, P., & Castaing-Lasvignottes, J. (1997). Development of a numerical sizing tool for a solid-gas thermochemical transformer -I. impact of the microscopic process on the dynamic behaviour of a solid-gas reactor. *Applied Thermal Engineering*, 17(6), 501-518.
- Ramachandran, P. A., & Doraiswamy, L. K. (1982). Modeling of noncatalytic gas-solid reactions. *AIChE Journal*, 28(6), 861-900.
- Smith, J.M. (1987). *Chemical Engineering Kinetics*. Singapore: McGraw-Hill Book Company
- Stitou, D., Goetz, V., & Spinner, B. (1997). A new analytical model for solid-gas thermochemical reactors based on thermophysical properties of the reactive medium. *Chemical Engineering and Processing*, 36, 29-43.
- Sørensen, R. Z., Hummelshøj, J. S., Klerke, A., Reves, J. B., Vegge, T., Nørskov, J. K., & Christensen, C. H. (2008). Indirect, Reversible High-Density Hydrogen Storage in Compact Metal Ammine Salts. *Journal of American Chemical Society*, 130, 8660-8668.
- Tosun, İ. (2015). *Thermodynamics Principles and Applications*. Singapore: World Scientific Publishing Pte.
- Wang, L., Wang, R., Wu, J., & Wang, K. (2004). Adsorption performances and refrigeration application of adsorption working pair of CaCl₂-NH₃. *Engineering and Material Science*, 47(2), 173-185. doi:10.1360/03ye0248.
- Wang, C., Zhang, P., & Wang, R. (2010). Performance of solid-gas reaction heat transformer system with gas valve control. *Chemical Engineering Science*, 65(10), 2910-2920. doi:10.1016/j.ces.2010.01.011
- Wongsuwan, W., Kumar, S., Neveu, P., Meunier, F., (2001). A review of chemical heat pump technology and applications. *Applied Thermal Engineering*, 21, 1489-1519. doi: 10.1016/S1359-4311(01)00022-9

Yake, D. E. (1980). Modeling of solid-gas reactions with application to the chlorination of lime (Unpublished master's thesis). Iowa State University.

$$u(19 - dr(18), 1) = u(19,1) - dr(18,1)u_x(19,1) + \frac{(dr(18,1))^2}{2!}u_{xx}(19,1) \quad \text{C6}$$

$$u(19 + dr(19), 1) = u(20,1) \quad \text{C7}$$

$$u(19 - dr(18), 1) = u(18,1) \quad \text{C8}$$

$$u(20,1) + u(18,1) \quad \text{C9}$$

$$= 2u(19,1) + u_x(19,1)[dr(19,1) - dr(18,1)] + u_{xx}(19,1)[(dr(19,1))^2 + (dr(18,1))^2] \cdot \frac{1}{2}$$

$$u_x(19,1) = \frac{u(20,1) - u(18,1)}{dr(19,1) + dr(18,1)} \quad \text{C10}$$

$$\frac{du^2}{dr^2} \quad \text{C11}$$

$$= \frac{u(20,1) - 2u(19,1) + u(18,1) - \left\{ \frac{u(20,1) - u(18,1)}{dr(19,1) + dr(18,1)} \right\}}{\left[\frac{(dr(19,1))^2 + (dr(18,1))^2}{2} \right]} \cdot (dr(19,1)$$

$$- dr(18,1))$$

D. Discretized Heat Transport Equation

$$\frac{d^2T}{dz^2} + S_{gen} = \rho_{sys} \cdot C_{p,sys} \cdot \frac{dT}{dt} \quad D1$$

When the Finite difference method is applied;

$$\begin{aligned} & k_{sys}^{(N-1,1)} \quad D2 \\ & \cdot \left[\frac{T^{(N,1)} - 2T^{(N-1,1)} + T^{(N-2,1)} - \left[\frac{T^{(N,1)} - T^{(N-2,1)}}{dz^{(N-1,1)} + dz^{(N-2,1)}} \right]}{\frac{[(dz^{(N-1,1)})^2 + (dz^{(N-2,1)})^2]}{2}} \cdot (dz^{(N-1,1)} \right. \\ & \left. - dz^{(N-2,1)}) \right] + 4N_{salt}^{(N-1,2)} \cdot \Delta H_{reaction} \cdot \frac{X^{(N-1,2)} - X^{(N-1,1)}}{dt} \\ & = \rho_{sys}^{(N-1,1)} \cdot C_{p,sys}^{(N-1,1)} \cdot \frac{T^{(N-1,2)} - T^{(N-1,1)}}{dt} \end{aligned}$$

Boundary Conditions for Energy Transport

$$at \ r = 0 \quad \frac{\partial T}{\partial r} = 0 \quad D3$$

Discretized form of Equation D3 is;

$$T(1,2) = T(2,2) \quad D4$$

Discretized form of Equation D5 becomes as given in Equation D6.

$$at \ r = R \quad -k_{sys} \frac{\partial T}{\partial r} = h_{NH_3} (T - T_{bulk}) \quad D5$$

$$T^{(N,2)} = \frac{k_{sys}^{(N-1,2)} \cdot T^{(N-2,2)} + [h_{NH_3}^1 \cdot (dz^{(N-1,2)} + dz^{(N-2,2)}) \cdot T_{sys}]}{k_{sys}^{(N-1,2)} + [h_{NH_3}^1 \cdot (dz^{(N-1,2)} + dz^{(N-2,2)})]} \quad D6$$

E. Discretized Mass Transport Equation

$$\begin{aligned}
 & \frac{D_{eff}^{N-1,2}}{T^{N-1,2}} \tag{E1} \\
 & \left[\frac{P_{NH_3}^{N,1} - 2P_{NH_3}^{N-1,1} + P_{NH_3}^{N-2,1} - \left[\frac{P_{NH_3}^{N,1} - P_{NH_3}^{N-2,1}}{dz^{N-1,2} - dz^{N-2,2}} \cdot (dz^{N-1,2} - dz^{N-2,2}) \right]}{\frac{(dz^{N-1,2})^2 + (dz^{N-2,2})^2}{2}} \right] \\
 & - \frac{2D_{eff}^{N-1,2}}{(T^{N-1,2})^2} \left[\frac{T^{N,2} - T^{N-1,2}}{dz^{(N-1,2)} + dz^{(N-2,2)}} \right] \left[\frac{P^{N,1} - P^{N-1,1}}{dz^{(N-1,2)} + dz^{(N-2,2)}} \right] \\
 & - \frac{D_{eff}^{N-1,2} P^{N-1,1}}{(T^{N-1,2})^2} \times \\
 & \left[\frac{T_{NH_3}^{N,2} - 2T_{NH_3}^{N-1,2} + T_{NH_3}^{N-2,2} - \left[\frac{T_{NH_3}^{N,2} - T_{NH_3}^{N-2,2}}{dz^{N-1,2} - dz^{N-2,2}} \cdot (dz^{N-1,2} - dz^{N-2,2}) \right]}{\frac{(dz^{N-1,2})^2 + (dz^{N-2,2})^2}{2}} \right] \\
 & + \frac{2D_{eff}^{N-1,2} P^{N-1,1}}{(T^{N-1,2})^3} \left[\frac{T^{N,2} - T^{N-1,2}}{dz^{(N-1,2)} + dz^{(N-2,2)}} \right]^2 \\
 & - 4N_{salt}^{(N-1,2)} \frac{dx}{dt} R_{gas} \\
 & = \frac{\varepsilon^{N-1,2}}{T^{N-1,2}} \left(\frac{P_{NH_3}^{N-1,2} - P_{NH_3}^{N-1,1}}{dt} \right) \\
 & - \frac{\varepsilon^{N-1,2} P_{NH_3}^{N-1,1}}{(T^{N-1,2})^2} \left(\frac{T^{N-1,2} - T^{N-1,1}}{dt} \right) \\
 & + \frac{P_{NH_3}^{N-1,1}}{T^{N-1,2}} \left(\frac{\varepsilon^{N-1,2} - \varepsilon^{N-1,1}}{dt} \right)
 \end{aligned}$$

F. Volume and Length Calculation of $\text{CaCl}_2 \cdot 2\text{NH}_3$ and $\text{CaCl}_2 \cdot 4\text{NH}_3$ Solid Pellet

The initial pellet volume can be calculated as given in Equation F1.

$$V_{\text{pellet, CaCl}_2} = \pi \cdot 0.007^2 \times 2 \times 10^{-3} = 3.08 \times 10^{-7} \text{ m}^3 \quad \text{F1}$$

The ratio between the molar volumes of CaCl_2 and $\text{CaCl}_2 \cdot 2\text{NH}_3$ and accordingly the volume and the length of the $\text{CaCl}_2 \cdot 2\text{NH}_3$ are given in Equations F2, F3, and F4.

$$\frac{MV_{\text{CaCl}_2 \cdot 2\text{NH}_3}}{MV_{\text{CaCl}_2}} = \frac{9.03 \times 10^{-5}}{5.10 \times 10^{-5}} = 1.76 \quad \text{F2}$$

$$V_{\text{pellet CaCl}_2 \cdot 2\text{NH}_3} = 3.08 \times 10^{-7} \times 1.76 = 5.42 \times 10^{-7} \text{ m}^3 \quad \text{F3}$$

$$L_{\text{pellet CaCl}_2 \cdot 2\text{NH}_3} = \frac{5.42 \times 10^{-7}}{\pi \times 0.007^2} = 3.52 \times 10^{-3} \text{ m} \quad \text{F4}$$

The ratio between the molar volumes of $\text{CaCl}_2 \cdot 2\text{NH}_3$ and $\text{CaCl}_2 \cdot 4\text{NH}_3$ and accordingly the volume and the length of the $\text{CaCl}_2 \cdot 4\text{NH}_3$ are given in Equations F5, F6, and F7.

$$\frac{MV_{\text{CaCl}_2 \cdot 4\text{NH}_3}}{MV_{\text{CaCl}_2 \cdot 2\text{NH}_3}} = \frac{1.29 \times 10^{-4}}{9.03 \times 10^{-5}} = 1.43 \quad \text{F5}$$

$$V_{\text{pellet CaCl}_2 \cdot 4\text{NH}_3} = 5.42 \times 10^{-7} \times 1.43 = 7.75 \times 10^{-7} \text{ m}^3 \quad \text{F6}$$

$$L_{\text{pellet CaCl}_2 \cdot 4\text{NH}_3} = \frac{7.75 \times 10^{-7}}{\pi \times 0.007^2} = 5.03 \times 10^{-3} \text{ m} \quad \text{F7}$$

G. MATLAB Code

```
clear all
clc
close all
%%
%Constant Values

cons.reactorvolume=0.0003225; %m^3
cons.ammonia=4.93*10^-10; %m
cons.gasconstant=8.314; %J/mol.K
cons.poredia=5*10^-8; %m
cons.alpha=1.1;
cons.beta=0.1;
cons.gama=0.85;
cons.Patm=100000; %Pa
cons.adsenthalpy=42268; %J/mol
cons.adsentropy=229.92; %J/mol.K
cons.a=34.236;
cons.b=-0.221*10^-1;
cons.c=1.231*10^-4;
cons.d=-1.088*10^-7;
cons.e=3.203*10^-11;
cons.g=9.81; %m/s^2
%%
%Initial Values
ini.adspreexponential=2.18E-9;
ini.despreexponential=0.0001;
ini.adsactivationenergy=-42000; %J/mol
ini.desactivationenergy=-13980; %J/mol
```

```

ini.Pbulk=193354; %Pa
ini.Tsys=318; %K
ini.grainradius=3*10^-5; %m
ini.graindiameter=ini.grainradius*2;
ini.pelletlength=1.76*10^-3; %m
ini.pelletx=0.007; %m
ini.pellettotallength=ini.pelletlength*2;
%ini.porosity=0.2;
%ini.tortuosity=ini.porosity^(-1);
ini.effectivediffusivity=2*10^-4; %%m^2/s
%%
%Initial values of physicochemical properties of the used materials
cons.reactantsaltMW=144.98; %g/mol
cons.reactantsaltdensity=1606; %kg/m^3
cons.reactantsaltCp=1352; %J/kg.K
cons.reactantsaltMV=9.02E-5; %m^3/mol
cons.reactantsaltTC=0.37; %W/m.K

cons.ammoniaMW=17; %g/mol
ini.ammoniadensity=(ini.Pbulk/(8.314*ini.Tsys))*17/1000; %kg/m^3
cons.ammoniaCp=(cons.a+cons.b*ini.Tsys+cons.c*ini.Tsys^2+cons.d*ini.Tsys^3+
cons.e*ini.Tsys^4)*(1000/17); %J/kg.K
cons.ammoniaTC=0.02493; %W/m.K
ini.ammoniadynamicviscosity=10.0258*10^-6; %Pa.s
ini.ammoniadynamicviscosityfilm=10.0258*10^-6; %Pa.s

cons.productsaltMW=178.98; %g/mol
cons.productdensity=1382; %kg/m^3
cons.productsaltCp=1676; %J/kg.K
cons.productsaltMV=0.000129; %m^3/mol

```

```

cons.productsaltTC=0.42; % W/m.K
%%
%Initial calculated values
ini.pelletvolume=pi*((ini.pelletx)^2)*(2*ini.pelletlength);
ini.equilibriumpressure=(exp((-
cons.adsenthalpy/(cons.gasconstant*ini.Tsys))+(cons.adsentropy/cons.gasconstant
)));
ini.adsrateconstant= ini.adspreexponential*exp(-
ini.adsactivationenergy/(cons.gasconstant*ini.Tsys));
ini.desrateconstant=ini.despreexponential*exp(-
ini.desactivationenergy/(cons.gasconstant*ini.Tsys));
ini.reactantsaltamount=0.587; %g
ini.porosity=0.1;
ini.availablevolume=cons.reactorvolume-ini.pelletvolume;
ini.ammoniamoleinreactor=(ini.Pbulk*ini.availablevolume)/(cons.gasconstant*ini.
Tsys);
ini.particlevolume=(4/3)*pi*(ini.grainradius)^3;
ini.particlenumber=ini.pelletvolume*(1-ini.porosity)/ini.particlevolume;

%%
%Finite Difference Method Starts
N=10;
ini.dz=ini.pelletlength/(N-1);
dt=2*10^-6;
z.Pammonia=zeros(N,2);
z.pelletvolumeincrement=zeros(N-1,2);
z.reactantmoleincrement=zeros(N-1,2);
z.productmoleincrement=zeros(N-1,2);
z.reactantmassincrement=zeros(N-1,2);
z.productmassincrement=zeros(N-1,2);

```

z.inireactantmoleincrement=zeros(N-1,2);
z.effectivediffusivity=zeros(N-1,2);
z.conversion=zeros(N-1,2);
z.unreactedsalt=zeros(N-1,2);
z.newpelletvolume=zeros(1,2);
z.diffusedammoniamole=zeros(1,2);
z.diffusedammoniapressure=zeros(1,2);
z.ammoniamoleinreactor=zeros(1,2);
z.graindiameter=zeros(1,2);
z.particlenumber=zeros(N-1,2);
z.consumedammonia=zeros(1,2);
z.consumedammoniadueto_reaction=zeros(N-1,2);
z.accumulationammoniaexcept_lastincrement=zeros(N-1,2);
z.lenghtincrementsummation=zeros(N-1,2);
z.T=zeros(N,2);
z.pelletdensity=zeros(N-1,2);
z.pelletCp=zeros(N-1,2);
z.pelletTC=zeros(N-1,2);
z.adsrateconstant=zeros(N-1,2);
z.desrateconstant=zeros(N-1,2);
z.equilibriumpressure=zeros(N,2);
z.convectiveHT=zeros(1,2);
z.newpelletlenght=zeros(1,2);
z.lenghtincrement=zeros((N-1),2);
z.solidvolumeincrement=zeros((N-1),2);
z.Pbulk=zeros(1,2);
z.availablevolume=zeros(1,2);
z.ammoniadensity=zeros((N-1),2);
z.ammoniaCp=zeros((N-1),2);
Ra=zeros(1,2);


```

Pr=zeros(1,2);
z.ammoniamass=zeros((N-1),2);
z.Tfilm=zeros(1,2);
z.ammoniaCpfilm=zeros(1,2);
A=zeros(1,2);
B=zeros(1,2);
Xammonia=zeros(1,2);
z.ammoniamoleincrement=zeros(N-1,2);

%%
% %% Initial conditions

z.Pammonia(1:(N),1)=ini.Pbulk;
z.equilibriumpressure(1:N,1)=ini.equilibriumpressure;
z.T(1:N,1)=ini.Tsys;
z.consumedammoniadueto_reaction(1:(N-1),1)=0;
z.accumulationammoniaexcept_lastincrement(1:(N-2),1)=0;
z.newpelletlength(1)=ini.pelletlength;
z.newpelletvolume(1)=ini.pelletvolume;
z.diffusedammoniapressure(1)=0;
z.consumedammonia(1)=0;
z.effectivediffusivity(1:(N-1),1)=ini.effectivediffusivity;
z.graindiameter(1:(N-1),1)=ini.graindiameter;
z.lengthincrement(1:(N-1),1)=ini.dz;
z.conversion(1:(N-1),1)=0;
z.adsrateconstant(1:(N-1),1)=ini.adsrateconstant;
z.desrateconstant(1:(N-1),1)=ini.desrateconstant;
z.pelletvolume(1)=ini.pelletvolume;
z.Pbulk(1)=ini.Pbulk;
z.availablevolume(1)=ini.availablevolume;

```

```

z.ammoniamoleinreactor(1)=ini.ammoniamoleinreactor;
z.ammoniadensity(1:(N-1),1)=ini.ammoniadensity;
z.ammoniaCp(1:(N-1),1)=cons.ammoniaCp;
z.ammoniadynamicviscosity(1:(N-1))=ini.ammoniadynamicviscosity;
z.Pr(1)=ini.ammoniadynamicviscosity*cons.ammoniaCp/cons.ammoniaTC;
z.Ra(1)=((cons.g*(1/ini.Tsys)*(z.T(N,1)-
ini.Tsys(1))*((pi*ini.pelletx*z.newpelletlength(1)))/(pi*ini.pelletx+2*z.newpelletl
enght(1)))^3)*(((z.ammoniadensity(1))^2)*z.ammoniaCp(1))/(((z.ammoniadynam
icviscosity(1))*(cons.ammoniaTC)));
z.Nu(1)=(0.825+((0.387*(z.Ra(1))^(1/6))/((1+(0.492/z.Pr(1))^(9/16))^(8/27))))^(2)
;
z.convectiveHT(1)=((z.Nu(1)*cons.ammoniaTC)*(pi*ini.pelletx+2*z.newpelletlen
ght(1)))/(pi*ini.pelletx*z.newpelletlength(1));
z.ammoniamass(1:(N-1),1)=ini.ammoniadensity*ini.porosity*ini.pelletvolume;
A(1)=0;
B(1)=0;

for iz=1:(N-1)
    z.lenghtincrementsummation(iz,1)=iz*(z.lenghtincrement(iz,1));
    z.pelletvolumeincrement(iz,1)=pi*((ini.pelletx)^2)*(z.lenghtincrement(iz,1));

z.reactantmassincrement(iz,1)=ini.reactantsaltamount*(z.pelletvolumeincrement(iz,
1)/ini.pelletvolume);
z.reactantmoleincrement(iz,1)=z.reactantmassincrement(iz,1)*(1/(110.98));
z.productmassincrement(iz,1)=0;
z.productmoleincrement(iz,1)=0;
z.solidvolumeincrement(iz,1)=z.pelletvolumeincrement(iz,1)*(1-ini.porosity);

z.particlenumber(iz,1)=(z.solidvolumeincrement(iz,1))/(((1/6)*pi*(z.graindiameter(
iz,1))^3));

```

```

z.pelletdensity(iz,1)=calculateinitialpelletdensity(iz, cons.reactantsaltdensity,
z.reactantmassincrement,cons.productdensity, z.ammoniadensity, ini.porosity,
z.productmassincrement);

```

```

z.pelletTC(iz,1)=calculateinitialpelletTC(iz, cons.reactantsaltdensity,
z.reactantmassincrement, cons.productdensity, ini.porosity,
z.productmassincrement, cons.reactantsaltTC, cons.productsaltTC,
cons.ammoniaTC);

```

```

z.pelletCp(iz,1)=calculateinitialpelletCp(iz, cons.reactantsaltdensity,
z.reactantmassincrement,cons.productdensity, ini.porosity,
z.productmassincrement, cons.reactantsaltCp, cons.productsaltCp, z.ammoniaCp);

```

```

z.unreactedsalt(iz,1)=
((z.reactantmoleincrement(iz,1))./(z.pelletvolumeincrement(iz,1)));
z.Pave1(iz,1)=(z.Pammonia(iz+1,1)+z.Pammonia(iz,1))/2;
z.Tave1(iz,1)=(z.T(iz+1,1)+z.T(iz,1))/2;

```

```

z.ammoniamoleincrement(iz,1)=(z.Pave1(iz,1)*z.pelletvolumeincrement(iz,1))/(co
ns.gasconstant*z.Tave1(iz,1));

```

```

end

```

```

z.inireactantmoleincrement(1:(N-1),1)=z.reactantmoleincrement(1:(N-1),1);

```

```

%%

```

```

% Time Loop Starts

```

```

tfinal=100000;

```

```

for j=0:dt:tfinal

```

```

    z.Pammonia(N,1)=z.Pbulk(1);

```

```

    for iz=1:(N-1)

```

```

z.conversion(iz,2)=calculateconversion(iz, z.conversion,dt, z.Pammonia,
ini.adspreexponential, ini.adsactivationenergy, cons.gasconstant, z.T, cons.alpha,
cons.beta, ini.despreexponential, ini.desactivationenergy, cons.gama);
if z.conversion(iz,2)>1
    z.conversion(iz,2)=1;
end
if z.conversion(iz,2)<0
    z.conversion(iz,2)=0;
end
end

for iz=1:(N-1)

z.productmoleincrement(iz,2)=z.inireactantmoleincrement(iz,1)*z.conversion(iz,2);
    z.reactantmoleincrement(iz,2)=z.inireactantmoleincrement(iz,1)-
z.productmoleincrement(iz,2);

z.reactantmassincrement(iz,2)=z.reactantmoleincrement(iz,2)*cons.reactantsaltMW
;

z.productmassincrement(iz,2)=z.productmoleincrement(iz,2)*cons.productsaltMW;
end

z.solidvolumeincrement(1:(N-1),2)=z.solidvolumeincrement(1:(N-
1),1).*(1+((cons.productsaltMV-cons.reactantsaltMV).*(z.conversion(1:(N-1),2)-
z.conversion(1:(N-1),1)))/cons.reactantsaltMV);
z.graindiameter(1:(N-1),2)=((((z.solidvolumeincrement(1:(N-
1),2))*6)/((z.particlenumber(1:(N-1),1))*(pi))).^(1/3));
z.pelletvolumeincrement(1:(N-1),2)=(z.solidvolumeincrement(1:(N-1),2))./(1-
(ini.porosity));

```

```

z.newpelletvolume(2)=2*sum(z.pelletvolumeincrement(:,2));
z.newpelletlength(2)=((z.newpelletvolume(2))/(pi*(ini.pelletx)^2))/2;
z.availablevolume(2)=cons.reactorvolume-z.newpelletvolume(2);
z.unreactedsalt(1:(N-1),2)=z.reactantmoleincrement(1:(N-
1),2)./(z.pelletvolumeincrement(1:(N-1),2));
z.sumvolumeincrement=cumsum(z.pelletvolumeincrement);
z.lengthincrementsummation(1:(N-1),2)=power(((z.sumvolumeincrement(1:(N-
1),2)))/(((ini.pelletx)^2)*pi),1);
z.lengthincrement(2:(N-1),2)=z.lengthincrementsummation(2:(N-1),2)-
z.lengthincrementsummation(1:(N-2),2);

z.lengthincrement(1,2)=power(((z.sumvolumeincrement(1,2)))/(((ini.pelletx)^2)*pi
),1);

%%
% Calculation of Local Temperature
for iz=2:(N-1)
    z.T(iz,2)=calculateT(z.T, iz, z.pelletTC, dt, z.pelletdensity, z.pelletCp,
z.lengthincrementsummation, z.lengthincrement, z.unreactedsalt, cons.adsenthalpy,
z.conversion, z.adsrateconstant, z.desrateconstant, z.equilibriumpressure,
z.Pammonia);
end
% Boundary Conditions for Energy Transport
z.T(1,2)=z.T(2,2);
z.T(N,2)=((z.pelletTC(N-1,1)*z.T(N-
2,2)+(z.convectiveHT(1)*ini.Tsys*(z.lengthincrement(N-
1,2)+z.lengthincrement(N-2,2)))/(z.pelletTC(N-
1,1)+(z.convectiveHT(1)*(z.lengthincrement(N-1,2)+z.lengthincrement(N-2,2))));
%%

```

% Calculation of Effective Diffusivity Based on New Porosity and Local Temperature Values

```
for iz=1:(N-1)
    z.effectivediffusivity(iz,2)=
z.effectivediffusivity(iz,1)*(((z.T(iz+1,2))+z.T(iz,2))/2)/(((z.T(iz+1,1))+z.T(iz,1
))/2))^(3/2);
```

```
end
```

```
%%
```

%Calculation of Local Pressure of Ammonia

```
for iz=2:(N-1)
    z.Pammonia(iz,2)=calculatePammonia(z.Pammonia, iz,
z.effectivediffusivity,z.lenghtincrementsummation, ini.porosity, z.lenghtincrement,
dt, z.T, z.conversion, z.unreactedsalt, cons.gasconstant);
```

```
end
```

```
z.Pammonia(1,2)=z.Pammonia(2,2);
```

```
for iz=1:N
    z.equilibriumpressure(iz, 2)=(exp((-
cons.adsenthalpy/(cons.gasconstant*z.T(iz,2)))+(cons.adsentropy/cons.gasconstant
)));
```

```
end
```

```
%%
```

%Calculation of Boundary Condition for Pressure of Ammonia

```
for iz=1:(N-1)
    z.consumedammoniadueto_reaction(iz,2)=((z.reactantmoleincrement(iz,1))-
(z.reactantmoleincrement(iz,2)))*2;
```

```
z.Pave1(iz,2)=(z.Pammonia(iz+1,2)+z.Pammonia(iz,2))/2;
```

```
z.Tave1(iz,2)=(z.T(iz+1,2)+z.T(iz,2))/2;
```

```

z.ammoniamoleincrement(iz,2)=(z.Pave1(iz,2)*z.pelletvolumeincrement(iz,2))/(cons.gasconstant*z.Tave1(iz,2));
    for iz=1:(N-2)
        z.accumulationammoniaexcept_lastincrement(iz,2)=((((z.Pammonia(iz,2))-
(z.Pammonia(iz,1)))+(z.Pammonia(iz+1,2))-
(z.Pammonia(iz+1,1)))/2)*(z.pelletvolumeincrement(iz,2))/(cons.gasconstant*ini.
Tsys);
    end
    A=2*sum(z.consumedammoniaaducto_reaction);
    B=2*sum(z.accumulationammoniaexcept_lastincrement);
    z.consumedammonia(2)=A(2)+B(2);
    z.ammoniamoleinreactor(2)=(z.ammoniamoleinreactor(1))-
(z.consumedammonia(2));

z.Pbulk(2)=(z.ammoniamoleinreactor(2))*cons.gasconstant*ini.Tsys/(ini.availablev
olume);
    z.Pammonia(N,2)=z.Pbulk(2);
    z.Xammonia(2)=1-(z.Pbulk(2)/ini.Pbulk);
    for iz=1:(N-1)

z.ammoniamass(iz,2)=((((z.Pammonia(iz,2)+z.Pammonia(iz+1,2))/2)*(z.pelletvolu
meincrement(iz,2))*((ini.porosity)))/(cons.gasconstant*((z.T(iz,2)+z.T(iz+1,2))/2))
)*(17/1000);

z.ammoniadensity(iz,2)=((((z.Pammonia(iz+1,2)+z.Pammonia(iz,2))/2))/(8.314*(z.
T(iz+1,2)+z.T(iz,2))/2))*17/1000; %kg/m^3
    end
    for iz=1:(N-1)

```

```

z.pelletdensity(iz,2)=calculatepelletdensity(iz, cons.reactantsaltdensity,
z.reactantmassincrement,cons.productdensity, z.ammoniadensity, ini.porosity,
z.productmassincrement);

```

```

z.pelletTC(iz,2)=calculatepelletTC(iz, cons.reactantsaltdensity,
z.reactantmassincrement,cons.productdensity, ini.porosity,
z.productmassincrement, cons.reactantsaltTC, cons.productsaltTC,
cons.ammoniaTC);

```

```

z.pelletCp(iz,2)=calculatepelletCp(iz, cons.reactantsaltdensity,
z.reactantmassincrement, cons.productdensity, ini.porosity,
z.productmassincrement, cons.reactantsaltCp, cons.productsaltCp,
cons.ammoniaCp);

```

```

end

```

```

%%

```

```

%Calculation of conductive heat transfer coefficient

```

```

z.Tfilm(2)=(ini.Tsys+z.T(N,2))/2;

```

```

z.ammoniadensityfilm(2)=(((z.Pammonia(N,2)+z.Pbulk(2))/2)/(8.314*(z.Tfilm(2)))
*17/1000);

```

```

z.ammoniaCpfilm(2)=(cons.a+cons.b*z.Tfilm(2)+cons.c*(z.Tfilm(2))^2+cons.d*(z
.Tfilm(2))^3+cons.e*(z.Tfilm(2))^4)*(1000/17);

```

```

z.Pr(2)=ini.ammoniadynamicviscosityfilm*z.ammoniaCpfilm(2)/cons.ammoniaTC
;

```

```

z.Ra(2)=((cons.g*(1/(z.T(iz+1,2)+z.T(iz,2))/2)*(z.T(N,1)-
ini.Tsys(1))*(z.newpelletlength(2))^3
*(((z.ammoniadensityfilm(2))^2*z.ammoniaCpfilm(2)))/(((ini.ammoniadynamicvi
scosityfilm(1))*(cons.ammoniaTC)))));

```


$$\text{Nu}(2) = (0.825 + ((0.387 * (\text{z.Ra}(2))^{(1/6)}) / ((1 + (0.492 / \text{z.Pr}(2))^{(9/16)})^{(8/27)})))^{(2)};$$

$$\text{z.convectiveHT}(2) = ((\text{Nu}(2) * \text{cons.ammoniaTC}) * (\text{ini.pelletx} + 2 * \text{z.newpelletlength}(2))) / (\text{ini.pelletx} * \text{z.newpelletlength}(2)));$$

%%

% Replace Old and New Values for the Next Time Step

$$\text{z.lengthincrement}(1:(\text{N}-1),1) = \text{z.lengthincrement}(1:(\text{N}-1),2);$$

$$\text{z.solidvolumeincrement}(1:(\text{N}-1),1) = \text{z.solidvolumeincrement}(1:(\text{N}-1),2);$$

$$\text{z.pelletvolumeincrement}(1:(\text{N}-1),1) = \text{z.pelletvolumeincrement}(1:(\text{N}-1),2);$$

$$\text{z.effectivediffusivity}(1:(\text{N}-1),1) = \text{z.effectivediffusivity}(1:(\text{N}-1),2);$$

$$\text{z.unreactedsalt}(1:(\text{N}-1),1) = \text{z.unreactedsalt}(1:(\text{N}-1),2);$$

$$\text{z.reactantmoleincrement}(1:(\text{N}-1),1) = \text{z.reactantmoleincrement}(1:(\text{N}-1),2);$$

$$\text{z.reactantmassincrement}(1:(\text{N}-1),1) = \text{z.reactantmassincrement}(1:(\text{N}-1),2);$$

$$\text{z.productmoleincrement}(1:(\text{N}-1),1) = \text{z.productmoleincrement}(1:(\text{N}-1),2);$$

$$\text{z.productmassincrement}(1:(\text{N}-1),1) = \text{z.productmassincrement}(1:(\text{N}-1),2);$$

$$\text{z.graindiameter}(1:(\text{N}-1),1) = \text{z.graindiameter}(1:(\text{N}-1),2);$$

$$\text{z.lengthincrementsummation}(1:(\text{N}-1),1) = \text{z.lengthincrementsummation}(1:(\text{N}-1),2);$$

$$\text{z.adsrateconstant}(1:(\text{N}-1),1) = \text{z.adsrateconstant}(1:(\text{N}-1),2);$$

$$\text{z.desrateconstant}(1:(\text{N}-1),1) = \text{z.desrateconstant}(1:(\text{N}-1),2);$$

$$\text{z.pelletCp}(1:(\text{N}-1),1) = \text{z.pelletCp}(1:(\text{N}-1),2);$$

$$\text{z.pelletdensity}(1:(\text{N}-1),1) = \text{z.pelletdensity}(1:(\text{N}-1),2);$$

$$\text{z.pelletTC}(1:(\text{N}-1),1) = \text{z.pelletTC}(1:(\text{N}-1),2);$$

$$\text{z.conversion}(1:(\text{N}-1),1) = \text{z.conversion}(1:(\text{N}-1),2);$$

$$\text{z.ammoniadensity}(1:(\text{N}-1),1) = \text{z.ammoniadensity}(1:(\text{N}-1),2);$$

$$\text{z.newpelletvolume}(1) = \text{z.newpelletvolume}(2);$$

$$\text{z.newpelletlength}(1) = \text{z.newpelletlength}(2);$$

$$\text{z.diffusedammoniapressure}(1) = \text{z.diffusedammoniapressure}(2);$$

```

z.diffusedammoniamole(1)=z.diffusedammoniamole(2);
z.availablevolume(1)=z.availablevolume(2);
z.Pbulk(1)=z.Pbulk(2);
z.convectiveHT(1)=z.convectiveHT(2);
z.ammoniamoleinreactor(1)=z.ammoniamoleinreactor(2);
Ra(1)=Ra(2);
Pr(1)=Pr(2);
Nu(1)=Nu(2);
z.Xammonia(1)=z.Xammonia(2);
z.Pammonia(1:N,1)=z.Pammonia(1:N,2);
z.equilibriumpressure(1:N,1)=z.equilibriumpressure(1:N,2);
z.T(1:N,1)=z.T(1:N,2);

```

```

if rem(j,1)==0

```

```

    T1=table(z.Pammonia(1:N,1), z.T(1:N,1), z.equilibriumpressure(1:N, 1),
'VariableNames',...
    {'Pammonia' 'T' 'equilibriumpressure'});

```

```

    T2=table(z.conversion(1:(N-1),1), z.lenghtincrement(1:(N-1),1),...
    z.effectivediffusivity(1:(N-1),1), z.adsrateconstant(1:(N-1),1),...
    z.desrateconstant(1:(N-1),1),...
    z.lenghtincrementsummation(1:(N-1),1), z.graindiameter(1:(N-1),1),...
    z.unreactedsalt(1:(N-1),1), z.reactantmoleincrement(1:(N-1),1),...
    z.productmoleincrement(1:(N-1),1),...
    'VariableNames', {'conversion' 'dr' 'Deff' 'adsrateconstant'
'desrateconstant'...
    'lenghtincrementsummation' 'dgrain' 'unreactedsalt'...
    'reactantmoleincrement' 'productmoleincrement'});

```

```

T3=table(z.Pbulk(1), z.newpelletvolume(1),z.newpelletlenght(1),...
        z.availablevolume(1),z.ammoniamoleinreactor(1), z.Xammonia(1),...
        'VariableNames',...
        {'Pbulk' 'newpelletvolume' 'newpelletlenght' 'availablevolume'...
        'ammoniamoleinreactor' 'Xammonia'});

filename = sprintf('z%04d.xlsx',j/1);
sheet1=1;
writetable(T1, filename, 'sheet', sheet1);
sheet2=2;
writetable(T2, filename, 'sheet', sheet2);
sheet3=3;
writetable(T3, filename, 'sheet', sheet3);
end
end
end

```

Calculation of conversion

function output=calculateconversion(iz, conversion,dt, Pammonia,
adspreexponential, adsactivationenergy, gasconstant,...

T, alpha, beta, despreexponential, desactivationenergy,
gama);

output=conversion(iz,1)+(dt/60)*(adspreexponential*exp(-
adsactivationenergy/(gasconstant*((T(iz+1,1)+T(iz,1))/2)))*(((Pammonia(iz+1,1)+
Pammonia(iz,1))/200000)^alpha)*((1-conversion(iz,1))^beta)-
despreexponential*exp(-
desactivationenergy/(gasconstant*((T(iz+1,1)+T(iz,1))/2)))*(conversion(iz,1)^gam
a));

Calculation of local Ammonia Pressure

function output8r=calculatePammonia(Pammonia, iz, effectivediffusivity, ...
lengthincrementsummation, porosity, lengthincrement, ...
dt, T, conversion, unreactedsalt, gasconstant);

A=

((2*dt*(effectivediffusivity(iz,2))/((porosity)*((lengthincrement(iz,2))+lengthinc
rement(iz-1,2)))*(((lengthincrement(iz,2))^2)+((lengthincrement(iz-
1,2))^2))))*(((Pammonia(iz+1,1))-(2*(Pammonia(iz,1)))+(Pammonia(iz-
1,1)))*((lengthincrement(iz,2))+lengthincrement(iz-1,2)))-(((Pammonia(iz+1,1))-
(Pammonia(iz-1,1)))*((lengthincrement(iz,2))-lengthincrement(iz-1,2))));

B= ((2*(effectivediffusivity(iz,2)*dt))/((porosity)*(T(iz,2)))*(((T(iz+1,2))-T(iz-
1,2)))/((lengthincrement(iz,2))+lengthincrement(iz-1,2)))*(((Pammonia(iz+1,1))-
(Pammonia(iz-1,1)))/((lengthincrement(iz,2))+lengthincrement(iz-1,2))));

C=

$$\begin{aligned} &(((2*\text{effectivediffusivity}(iz,2))*\text{Pammonia}(iz,1))*dt)/((T(iz,2))*(\text{porosity})*(\text{lenght} \\ &\text{increment}(iz,2))+(\text{lenghtincrement}(iz- \\ &1,2)))*(((\text{lenghtincrement}(iz,2))^2)+((\text{lenghtincrement}(iz- \\ &1,2))^2))))*(((T(iz+1,2))-(2*(T(iz,2)))+(T(iz- \\ &1,2)))*((\text{lenghtincrement}(iz,2))+(\text{lenghtincrement}(iz-1,2))))-(((T(iz+1,2))-(T(iz- \\ &1,2)))*((\text{lenghtincrement}(iz,2))-(\text{lenghtincrement}(iz-1,2)))))); \end{aligned}$$

D=

$$\begin{aligned} &(((2*(\text{effectivediffusivity}(iz,2))*dt*(\text{Pammonia}(iz,1)))/(((T(iz,2))^2)*(\text{porosity}))))* \\ &((((T(iz+1,2))-(T(iz-1,2)))/((\text{lenghtincrement}(iz,2))+(\text{lenghtincrement}(iz- \\ &1,2))))))^2); \end{aligned}$$

$$E= ((4*(\text{unreactedsalt}(iz,2))*\text{gasconstant}*(T(iz,2))/(\text{porosity}))*((\text{conversion}(iz,2))- \\ (\text{conversion}(iz,1))));$$

$$F= \text{Pammonia}(iz,1);$$

$$G= (((\text{Pammonia}(iz,1))/(T(iz,2)))*((T(iz,2))-(T(iz,1))));$$

$$\text{output}\&r=A-B-C+D-E+F+G;$$

Calculation of local temperature

function output7r=calculateT(T, iz, pelletTC, dt, pelletdensity, pelletCp,lenghtincrementsummation, lenghtincrement, unreactedsalt, adsenthalpy, conversion, adsrateconstant, desrateconstant, equilibriumpressure, Pammonia);

A=

$$((2*\text{pelletTC}(iz,1)*dt)/(\text{pelletdensity}(iz,1)*\text{pelletCp}(iz,1)*(\text{lenghtincrement}(iz,2))+1$$

```

enghtincrement(iz-1,2))*(((lenghtincrement(iz,2))^2)+(lenghtincrement(iz-
1,2))^2))*(((T(iz+1,1)-2*T(iz,1)+T(iz-
1,1))*(lenghtincrement(iz,2)+lenghtincrement(iz-1,2)))-((T(iz+1,1)-T(iz-
1,1))*(lenghtincrement(iz,2)-lenghtincrement(iz-1,2)))));

```

```

B=((4*unreactedsalt(iz,2)*adsenthalpy)/(pelletdensity(iz,1)*pelletCp(iz,1))*(conv
ersion(iz,2)-conversion(iz,1)));

```

```

C= T(iz,1);

```

```

output7r=A+B+C;

```

Calculate pellet thermal conductivity

```

function output_6=calculatepelletCp (iz, reactantsaltdensity,
reactantmassincrement,productdensity, porosity, productmassincrement,
reactantsaltCp, productsaltCp, ammoniaCp);
output_6=reactantsaltCp*(((reactantmassincrement(iz,2))/reactantsaltdensity)/(((rea
ctantmassincrement(iz,2))/reactantsaltdensity)+((productmassincrement(iz,2))/prod
uctdensity)))+ammoniaCp.*porosity+productsaltCp*(((productmassincrement(iz,2)
)/productdensity)/(((reactantmassincrement(iz,2))/reactantsaltdensity)+((productma
ssincrement(iz,2))/productdensity)));

```

Calculate pellet density

```

function output_4=calculatepelletdensity(iz, reactantsaltdensity,
reactantmassincrement,productdensity, ammoniadensity, porosity,
productmassincrement);

```

```

output_4=reactantsaltdensity*(((reactantmassincrement(iz,2))/reactantsaltdensity)/((
(reactantmassincrement(iz,2))/reactantsaltdensity)+((productmassincrement(iz,2))/
productdensity)))+ammoniadensity(iz,2).*porosity+productdensity*(((productmass

```

```
increment(iz,2)/productdensity)/(((reactantmassincrement(iz,2))/reactantsaltdensity)+((productmassincrement(iz,2))/productdensity))));
```

```
function output_5=calculatepelletTCv (iz, reactantsaltdensity,  
reactantmassincrement, productdensity, porosity, productmassincrement,  
reactantsaltTC, productsaltTC, ammoniaTC);  
output_5=reactantsaltTC*(((reactantmassincrement(iz,2))/reactantsaltdensity)/(((reactantmassincrement(iz,2))/reactantsaltdensity)+((productmassincrement(iz,2))/productdensity)))+ammoniaTC*porosity+productsaltTC*(((productmassincrement(iz,2))/productdensity)/(((reactantmassincrement(iz,2))/reactantsaltdensity)+((productmassincrement(iz,2))/productdensity))));
```


CURRICULUM VITAE

Surname, Name: Karakaş Helvacı, Zeynep

EDUCATION

Degree	Institution	Year of Graduation
MS	METU Chemical Engineering	2016
BS	METU Chemical Engineering	2013
High School	Gölbaşı Anatolilan High School, Ankara	2007

FOREIGN LANGUAGES

Advanced English.

PROFESSIONAL EXPERIENCE

Process Engineer at Roketsan A.Ş. (2019 – Ongoing)

Teaching Assistant at METU, Chemical Engineering Department (2014-2019)

PUBLICATIONS

- International Congress of Chemical and Process Engineering - CHISA - PRAG - 2016

Oral Presentation on Theoretical and Experimental Investigation of Ultrasound Propagation Through Porous Medium

- 4th Anatolian School of Catalysis - İzmir - 2016

Poster Presentation on Investigation of Ammonia Adsorption/Desorption Systems of Alkaline Earth Metal Salts

- 7th Catalysis Conference -Denizli- 2018

Poster Presentation on Theoretical Investigation of Adsorption/Desorption Reaction between Metal Salts and Ammonia Based on “Unreacted Shrinking Core” Model.

- 9th Eastern Mediterranean Chemical Engineering Conference -Ankara- 2018

Poster Presentation on Theoretical Investigation of Structural Changes during Ammonia Adsorption Reactions of Metal Salts

- 8th National Catalysis Conference -Ankara- 2021

Poster Presentation on Theoretical and Experimental Investigation of Metal Salt-Ammonia Reactive System